The Specialist Committee on Validation of Waterjet Test Procedures

Final Report and Recommendations to the 24th ITTC

1. INTRODUCTION

1.1 Membership and Meetings

The 23rd ITTC appointed the Specialist Committee on Validation of Waterjet Test Procedures with the following Membership:

- Prof. Tom Van Terwisga (Chairman).
  Maritime Research Institute Netherlands and Delft University of Technology, The Netherlands.
- Dr. Daniele Ranocchia (Secretary).
  Istituto Nazionale per Studi ed Esperienze di Architettura Navale, Italy.
- Mr. John George Hoyt III.
  Naval Surface Warfare Center, Carderock Division, U.S.A.
- Mr. Reima Aartojärvi.
  Rolls-Royce AB - Hydrodynamic Research Center, Sweden.
- Prof. Ho Hwan Chun.
  Pusan National University, Korea.
- Mrs. Elena Semionycheva.
  Krylov Research Institute, Russia.
- Prof. Mehrdad Zangeneh.
  University College London, United Kingdom.

Mr. Alan Becnel (Naval Surface Warfare Center, Carderock Division, U.S.A.) attended the meetings as an observer, in which he made a vital contribution to both the coordination and the analysis of the ITTC work related to the GCRMTC project.

Four meetings were held as follows:

- Pusan National University, Korea, December 2002.
- Ischia, Italy, October 2003.
- University College London, United Kingdom, May 2004.
- Amphibious Vehicle Test Branch, U.S.A., January 2005.

At the first meeting of the Committee Dr. Daniele Ranocchia was elected Secretary of the Committee. Responsibilities for the coordination of the various standardization tests were delegated as follows:

- Self-propulsion Tests - Dr. Daniele Ranocchia.
- Pump and Waterjet System Tests - Mr. Reima Aartojärvi.

1.2 Introduction

The objective of the Specialist Committee on Validation of Waterjet Test Procedures is to provide proven procedures for the determination of the powering characteristics of waterjet propelled vessels. The objective includes an uncertainty study for the prediction of the main powering characteristics that can be derived

from propulsion tests, such as jet thrust and effective jet system power.

To meet this objective, the theoretical framework proposed by the Specialist Committee on Waterjets to the 21st ITTC was scrutinized and elaborated. A description of the resulting theoretical model for the prediction of powering characteristics of jet propelled vessels is presented in Section 3. Secondly, to collect results of several alternative experimental methods, a series of standardization tests has been designed and has been conducted by several ITTC Members. The various results were analysed and evaluated on simplicity and uncertainty.

Three types of tests were conducted:

- Self-propulsion tests with the aim to determine the required flow rate, jet thrust and effective jet system power, including jet-hull interaction factors. To this end, a model of a high speed displacement monohull driven by two waterjets was tested.
- Waterjet System Tests with the aim to determine the system characteristics in terms of flow rate, head and torque, and in terms of required power.
- Pump tests with the aim to determine the hydraulic characteristics of the pump without the flow distortion caused by the intake and hull boundary layer.

An extensive description of each of the three tests is given in Hoyt et al. (1999).

These tests were recommended by the 22nd ITTC "Specialist Committee on Waterjets" and accepted by the Conference. The 23rd and 24th ITTC "Specialist Committees on the Validation of Waterjet Test Procedures" were tasked to carry out the corresponding work.

Validation of the Waterjet Test Procedures has become possible by teaming up with a three year project, sponsored by the United States Office of Naval Research (ONR). This project is administrated by the Gulf Coast Region Maritime Technology Center (GCRMTC), situated at the University of New Orleans. The GCRMTC Project has provided two hull models with representative stock jets and intakes, as well as one scaled waterjet model. The GCRMTC Project will in the following be referred to as "Gulf Coast Project".

As pointed out by the 22nd ITTC Committee on Waterjets, the scope of the current standardization effort is limited to the determination of the powering characteristics of the waterjet driven vessel, including determination of the characteristics of its components. The emphasis is thereby on experimental procedures, although the theoretical framework is designed such that it offers a model for empirical prediction. This means that when sufficient data are collected, a computed estimate of the powering characteristics can be given.

The effect of cavitation on the powering characteristics and possible erosion effects is deliberately left out of the scope, as this was regarded to disclose a whole new problem area. It is assumed in the work of our Committee that the possible cavitation that may occur in the pump or in the intake during operation of the vessel, does not affect the powering characteristics. This seems to be a realistic assumption for most vessels in operation, but should nevertheless be checked with the jet manufacturer for each individual application.

Another issue in the definition of the scope of the Committee's work is the introduction of a number of propulsor concepts that could be situated in between the open shaft propeller and the 'conventional' waterjet. One can think in this respect of other so called 'hull integrated propulsors', completely or partly surrounded by the hull, and of the so called ventilated waterjet. It was decided by the previous Specialist Committee, in consultation with the Propulsion Committee of the 23rd ITTC, to limit this work to non ventilated hull integrated propulsors, of which the conventional waterjet is the most important example.

This report first gives an update of the relevant literature that has been published in the tenure of the current Committee. Chapter 3 subsequently deals with the theoretical model that is used in the performance prediction. The Chapters 4 and 5 deal with the results of the self-propulsion tests and the pump and waterjet system tests respectively. Finally, Chapter 6 yields the conclusions and recommendations.

2. LITERATURE UPDATE

This review presents an update of the literature released since the 23rd ITTC, which was held in September of 2002.

The literature review is constrained to an update of CFD analysis, design and performance prediction, design of inlet duct, experiment and study on axial flow type waterjet.

These are the main topics being addressed in the literature during the last three years. The momentum flux method (Kruppa et al., 1996) is still being practised for model tests. There are not many papers related to the analysis of model tests while there are some on the computation with CFD techniques in the past three years.

Major sources contributing to the present literature on waterjet propulsion are the International Conference on Waterjet Propulsion 4, organized by the RINA in London in May, 2004 and the 2nd PNU International Colloquium on Waterjets in Busan, December 2002.

2.1 Inlet Duct

Park et al. (2002a) analyze the flow around an intake by using a sliding multi-block method. The computed velocities and pressures are compared with the experimental results from wind tunnel tests under the same condition. The computational domain is chosen large enough so as not to influence the inflow velocity by a boundary grid. The computations and experiments are conducted for varying *NVR* values. A fair agreement is found between them.

Park et al. (2002b) analyze the intake flow of a mixed flow type waterjet with an in-house developed code which uses the cell-centred finite volume method with QUICK scheme. Three kinds of intake shapes, whose main difference is in the inlet breadth, are designed and computed. The computed results show that a large difference in the performance of each intake is found and that this difference increased with increasing Intake Velocity Ratio *IVR*. The authors conclude that the CFD code is a very useful tool in the initial design process of a waterjet duct shape.

Choi et al. (2002) also describe a generation technique for an inlet geometry by using NURBS. The authors state that an excellent smooth surface for a duct can be obtained by this NURBS method.

A “loft and blending technique” is applied to the modelling of a waterjet intake duct by Park et al. (2002c). Parametric design methodology which includes main dimensions, section shapes and characteristic parameters such as Section Area Curve (SAC), Slope curve and Chine line is also used for the systematic design of smooth duct surfaces.

Research for an optimum inlet geometry for three different kinds of vessels is conducted by Bulten and Verbeek (2003). The computation by the developed CFD code is used for an optimization of the inlet geometry. The authors conclude that the vessel specific optimization of inlet geometry significantly improves the performance of the waterjet system compared to the non-optimum case.

Wilson et al. (2004) study the effect of inlet shape by a variation of four kinds of shape. Measurements are boundary layer thickness, captured area, wake width, etc. The experimental results show that the simple rectangular shape is good enough although the typical con-

figuration of an elliptic type is the best in scalloped capture area point of view.

2.2 Waterjet System

Park et al. (2002d) apply a developed in-house code to a flush type axial flow waterjet system. An iterative time marching method and a sliding multi-block method are used in the analysis program. The computed pressures on the inside of the duct are compared with the experimental results, which show an excellent agreement between them.

The computed jet velocities just behind the nozzle are also compared with the measured velocity, which again shows a good correlation with the experiments.

Bulten and Verbeek (2004) also use a commercial code which has been developed with a steady-state multiple frame of reference (MFR) approach and with a fully transient moving mesh method, whose computed results are validated by a comparison with experimental data.

The authors conclude that the developed code with an MFR approach has a very good accuracy in the computation of thrust and torque of the impeller. Furthermore, the unsteady transient computation gives more insight in the pressure fluctuations.

The PIV measuring technique that is recently used in various fields, is applied to measure the flow velocity around the inlet and nozzle area of an axial flow type waterjet in a wind tunnel by Kim et al. (2002). The experimental data in terms of velocities and pressures in the whole domain of the inner duct surface is rare because it is difficult to set up the beam position to cover the complete flow domain. The pressure distributions are also measured by scanning a pressure transducer along the duct inside. Kim et al. (2002) conclude that the difference of flow phenomena is not large for a variation of *NVR*. This conclusion is rather different from the computational findings by Park et al. (2002), which may be attributed to the difference in the experimental condition and the waterjet type.

Kooiker et al. (2003) present results of jet system tests on a waterjet that is mounted on top of a cavitation tunnel. The authors measured pump performance and jet system performance and compared the results to measurements on a pump in a typical pump loop test, where the pump loop test on a larger scale model showed a 2% lower pump efficiency. They concluded that the intake working point, expressed in IVR value, does have a significant effect on pump performance due to the variations in velocity profile at the pump face (up to some 5% in pump efficiency for the lightest loading tested). The sensitivity of pump performance for varying intake performance was confirmed with the sensitivity of cavitation inception number for variations in the intake operating point.

Murrin et al. (2004) propose the wind tunnel test for a large scale waterjet test by increasing model size to predict the performance accurately. The authors emphasize that their measurements can be very accurate and convenient on a large model. The test results are validated with CFD results and a good agreement is generally found.

Carlton (2002) describes some recent full scale experience by Lloyd's Register. He focuses on the actual failure problems in a full scale waterjet system which occurs on occasions for a variety of reasons. The waterjet intake and duct are a main source for failure problems due to flow separation and cavitation. The impeller and stator is another important factor in failure problems, related to vibration and cavitation which cause problems in the connection between the waterjet units and the ship's hull. The author also mentions the relation between course keeping and manoeuvring and waterjet hull connection problems, which are also related to the previously mentioned problems.

2.3 Pump Design and Performance Analysis

Facinelli et al. (2003) describe the design of a waterjet as an iterative process, using a variety of codes. The preliminary design is first conducted with the code based on a streamline theory. The more detail design is then conducted with the potential based program (TURBOdesign). The viscous effect is finally included by the CFD code (CFX-TASCflow). The authors conclude that the waterjet iteratively designed by the various analysis codes has a better performance compared to the waterjet no iteratively designed using a single code.

CFD computation are applied to the design of an axial flow type waterjet. Kim et al. (2003) use the CFD analysis code for the optimum design of a waterjet system by an iteration technique. The detailed computation of pressure distribution on impeller blade surface and computed streamlines are used for the optimum design of stator and impeller as well.

2.4 System Design and Performance Prediction

Aartojärvi et al. (2004) and Seil (2001) describe an analysis of a steering and reversing unit by using the commercial Fluent code. This research is motivated by the development of a lighter steering and reversing unit for very large waterjet systems. It was difficult to analyze this kind of device, due to its complex configuration. With the progress of grid generation techniques and computer power, this kind problem can nowadays be solved. The developed CFD program validates the performance of the newly designed control device. The computed loads on a waterjet surface are also used as hydrodynamic input data for the computation of stresses in the waterjet system through an FE analysis.

Buckingham (2004) uses another commercial tool for the assessment of candidate propulsion options. The so called Ptool well provides the modelling of a waterjet of different size conveniently by the use of a non-dimensional method.

Altosole et al. (2004) describe the performance prediction by using dynamic numerical simulation which is developed for the analysis of unsteady transient performances. Individual blocks are used for the analysis of the hull, the prime mover, the gearbox and the pump, which are connected with each other in a way which takes interaction into account. This approach being similar to the multi-block method.

The numerical model has been developed in a Matlab-Simulink software environment but a detailed description is omitted.

Wang et al. (2004) describe the relation between power absorption and vessel speed for a waterjet system in actual ship operation. They report that the power absorption of the waterjet, which is normally proportional to the cube of speed of revolution, is less dependent on the vessel speed than in the case of a conventional screw propeller. This waterjet property prevents an engine to reach the overload condition, even at a sudden acceleration to a full speed.

Another study on the tradeoffs between two and three waterjets is conducted by Bowles et al. (2004). This study is focused on the OPC (overall performance coefficient) as a function of the number of waterjets. They conclude that the difference in OPC due to the difference of arrangement is small. An only slight improvement can be achieved by increasing the unit waterjet size. Therefore, it is concluded that the improvement in waterjet OPC through the selection of different waterjet combinations and size is insignificant as long as the design condition and power remain the same.

Verbeek (2002) describes waterjet concepts for especially large fast ships. The basic concepts of efficiency, inlet design and mechanical design are reviewed and he concludes that the basic concepts as used in small ships can be

used for large fast ships. Units up to 75000 kW power can be produced with today's technology, in which case the production technology might be the limiting factor.

A review of the Gulf Coast waterjet project is presented by Wilson et al. (2003). The review addresses the development and validation of prediction tools for the design, computational evaluation and experimental assessment of a specific application of waterjet propulsion for a small Navy ship. A valuable correlation study for the model and its full scale version has been made.

The velocity profile in the capture area is quite different for model and full scale ship, due to the viscous effects as was expected. An analysis of the non-uniformity at each station of the duct is also conducted to verify its effect for the model as well as the full scale ship. The results do not differ much from the uniform flow case.

Chun et al. (2003) describe a self-propulsion test and subsequent analysis using the momentum flux method (Kruppa et al., 1996) and propulsive factor method (Savitsky et al., 1987). These tests are made to predict the performance of an amphibious tracked vehicle with two axial flow type waterjets. The predicted effective powers by the two methods appear not to differ much. The authors conclude that this fact is attributed to the fact that the trim of the model is almost the same for the resistance and the self-propulsion tests. It seems difficult to predict the full-scale OPC from the model test because the pump efficiency can not be accurately predicted due to the presence of scale effects. A full-scale bollard pull and sea trial test is anticipated and these results should be used to learn more about the scale effects in OPC.

Kim et al. (2004) present the results of a study on a Pod type waterjet system for an amphibious wheeled vehicle. In the case of a short Pod type waterjet, which is rather similar to a ducted propeller, it is difficult to evaluate the model test results by the momentum flux method because the station numbers were originally defined for a flush type waterjet system. The authors propose that the Capture Area and velocity field around inlet region be measured in detail for an accurate analysis of the model test. Although the capture area and the definition of stations are roughly estimated, there is no large difference between the predicted value by the ITTC '96 momentum method Kruppa et al. (1996) and the propulsive factor method by Savitsky et al. (1987).

3. POWERING PERFORMANCE PREDICTION

The proposed procedure for a prediction of the powering performance of a waterjet driven vessel is based on a modular approach in testing and analysis. The advantage of this approach is manifold:

- The analysis procedure is in harmony with the engineering approach in the design of these vessels; A suitable waterjet is typically selected for a given hull form.
- The testing procedure thus allows for a black box approach, allowing the use of a stock pump as a model for the pump of the prototype waterjet.
- Responsibilities for delivery and quality of data are easily defined.

The method proposed here is an elaboration of an earlier method, designated "momentum flux method", that was already proposed by the Specialist Committee on Waterjets to the 21st ITTC (Kruppa et al., 1996). This Committee discussed two distinct methods; The so called "momentum flux method" and the "direct thrust measurement" method.

The most important advantages of the "momentum flux method" are that a suitable arbitrary pump can be used to provide the required flow rate (corresponding to required thrust), and that no complicated watertight sealing between the waterjet system and the

hull is needed. Another advantage is that the scale of the waterjet model can be chosen smaller in the first method, as internal scale effects do not matter. An advantage of the "direct thrust measurement" method is that the jet system performance need not be measured separately, as this is implicitly taken into account by the correct scale model.

Although it was attempted from the beginning by the successive Waterjet Committees to include tests following the "direct thrust measurement" method, in the end no institute was willing to conduct these.

From the experience of the Committee Members with this method, it was concluded that this method is expensive and cumbersome. For the above reasons, the Committee has focused on the momentum flux method.

The main differences with the method proposed by the Waterjet Committee of the 21st ITTC are:

- distinction between momentum and energy fluxes,
- relation between bare hull resistance and waterjet net thrust,
- improved procedures for the determination of ingested and discharged momentum,
- determination of tow force,
- experience based advise on flow rate measurement,
- matching procedure between self-propulsion test results and waterjet system performance.

3.1 Systems Decomposition

In decomposing a complex system, the mutual relations and constraints between the subsystems should be properly described in order not to change the characteristics of the overall system. This implies that system boundaries and the flow parameters at these boundaries should be defined carefully.

The waterjet-hull system is decomposed into a bare hull and a waterjet system. The bare hull is equal to the hull of the combined system with the exception that the waterjet is not present. The weight and the position of the Centre of Gravity correspond to those of the combined system in operation. This definition is in line with the proposed 1987 ITTC Procedure (Savitsky et al., 1987).

The waterjet system can be subdivided into a pump and a ducting system. The pump is the driving heart of the waterjet, converting mechanical power (input) into hydraulic power (output). The ducting system leads the required flow from the exterior to the pump and through the nozzle, back into the environment.

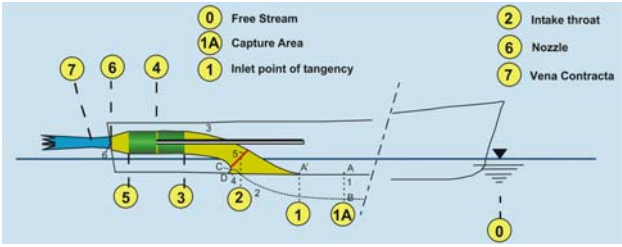

Figure 3.1- Control volume representing the hydrodynamic model of the waterjet.

A suitable control volume needs to be selected for the waterjet system in order to be able to compute or determine the powering characteristics from measurements. Considerations in the choice of the boundaries of the control volume are:

- The momentum and energy fluxes going through the boundaries of the system should be easy to measure or compute.
- The flow that is largely governed by the jet system should belong to this system
- The protruding part of the control volume (ABC in Fig. 3.1) should be as small as possible to avoid strong interaction effects with the external flow.

The Control Volume that is defined by the stream-tube captured in between stations 1A and 6 is selected as the volume that meets the above criteria best. This control volume is

essentially the same as the one used by the 21st ITTC Waterjet Committee (1996). The ducting system is partly defined by the material (fixed) boundaries of the jet system, partly by a dividing stream surface BC ahead of the physical intake opening A'D (Fig. 3.1). This dividing stream surface (designated A_2) is an imaginary surface in the flow, through which no transport of mass occurs by definition.

The imaginary capture area A_1 is positioned slightly forward of the intake's ramp tangency point (A'). This position is selected to avoid major flow distortions by the intake geometry. A distance of one impeller diameter in front of the ramp tangency point seems a practical choice.

Point D is determined by the intake geometry and is referred to as 'outer lip tangency point'.

The geometry of the surfaces A_1 and A_2 depends on the point of operation of the waterjet. It may also be affected by the external flow, e.g. in the case where a longitudinal pressure gradient exists.

The flow is discharged through the nozzle. The nozzle face (Station 6) is recommended here as the exit area of the control volume, in lieu of the vena contracta (Station 7) for practical reasons. In the vast majority of the cases, the diameter of the vena contracta is approximately the same as the nozzle exit diameter. This latter diameter can be measured accurately, whereas the vena contracta is difficult to measure. Possible errors due to this assumption can be cancelled by applying a bollard pull calibration procedure, where the relation between flow rate measurement and jet thrust is determined.

The flow is further bounded by area 3, representing the physical ducting of the waterjet system. All forces, including pump forces, exerted by the waterjet system on the hull can only be passed through this area, and through the pump housing and shaft.

3.2 Description of Powering Characteristics

A comprehensive way to express the powering performance of any propulsor is through its non dimensional effective power, expressed in efficiency:

$$\eta = \frac{P_{\text{out eff}}}{P_{\text{in}}} \tag{3.1}$$

where,
$P_{\text{out eff}}$ = effective power delivered by system
P_{in} = power input in system;
$P_{\text{in}} = P_{\text{out eff}} + P_{\text{loss}}$
P_{loss} = power losses

The process of energy conversion by each subsystem and the respective efficiencies are sketched in Fig. 3.2.

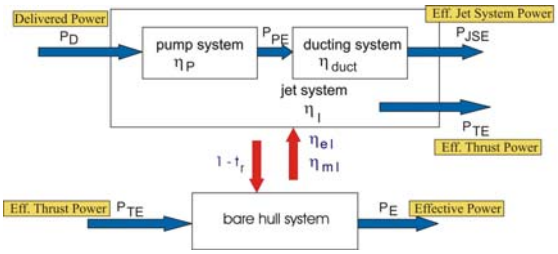

Figure 3.2- Energy conversion through waterjet-hull system and subsystems.

When two distinct subsystems are combined, there are often interactions. For the purpose of design or analysis of such a combined system, it is desirable to have the interaction explicitly defined. The overall efficiency of the combined system can then be obtained from the "free stream efficiency" η_0 and an interaction efficiency η_{INT}, according to:

$$\eta_{\text{D}} = \eta_0 \eta_{\text{INT}} \tag{3.2}$$

This approach is similar to that adopted for the ITTC propeller propulsion model.

The energy conversion processes which are affected by the waterjet-hull interface are

derived in separate equations for all components, viz.:

- the jet system's effective thrust power P_{TE}, affected by modified momentum fluxes;
- the Jet System Effective (hydraulic) power P_{JSE} which is affected by the energy fluxes at the interface and the nozzle sinkage;
- and the hull resistance which is affected by the changing flow pattern over the aftbody.

The hull-jet interaction effects in these quantities can be quantified as the ratio of the power in free stream conditions to that power in operational conditions at equal flow rate Q:

$$\eta_{kI} = \frac{P_{free\ stream}}{P_{operational}} = \frac{P_{k0}}{P_k} \tag{3.3}$$

where,
the subscript k indicates the specific power component that is affected by interaction: Either Effective Jet System Power P_{JSE} or Effective Thrust Power P_{TE}.

The overall efficiency of the combined waterjet-hull system is, in line with the definition in Eq. 3.1, given by:

$$\eta_D = \frac{P_E}{P_D} = \frac{R_{TBH} U_0}{P_D} \tag{3.4}$$

Expressing the overall efficiency as the product of the various efficiencies of the subsystems and allowing for the interaction terms discussed above, yields:

$$\eta_D = \frac{P_E}{P_{TE}} \frac{P_{TE}}{P_{TE0}} \frac{P_{TE0}}{P_{JSE0}} \frac{P_{JSE0}}{P_{JSE}} \frac{P_{JSE}}{P_{PE}} \frac{P_{PE}}{P_D} \tag{3.5}$$

Considering the subsystems defined in Fig. 3.2, the respective subsystem efficiencies following Eq. 3.1, are given by:

- Thrust Deduction

$$(1-t) = \frac{P_E}{P_{TE}} = \frac{R_{BH}}{T_{net}} \tag{3.6}$$

- Momentum Interaction

$$\frac{1}{\eta_{mI}} = \frac{P_{TE}}{P_{TE0}} = \frac{T_{net}}{T_{net0}} \tag{3.7}$$

- Ideal Jet Efficiency

$$\eta_I = \frac{P_{TE0}}{P_{JSE0}} = \frac{T_{net0} U_0}{QH_{JSE0}} = \frac{\Delta \overline{M}_x U_0}{E_7 - E_0} \tag{3.8}$$

- Energy Interaction

$$\eta_{eI} = \frac{P_{JSE0}}{P_{JSE}} = \frac{E_7 - E_0}{E_7 - E_1} \tag{3.9}$$

- Ducting Efficiency

$$\eta_{duct} = \frac{P_{JSE}}{P_{PE}} \tag{3.10}$$

- Pump Efficiency

$$\eta_P = \frac{P_{PE}}{P_D} \tag{3.11}$$

An elaboration of the above efficiency terms will be given in the following.

Jet System. Important advantages of the introduction of "free stream characteristics" for the isolated jet system, is that the several jet system performances can be compared with each other and the so called jet efficiency (defined by Eq. 3.8) reduces to a simple form (referred to as the ideal efficiency η_I).

The free stream jet efficiency η_0 can be written as the product of the ideal efficiency (accounting for the axial kinetic energy losses), the ducting efficiency (accounting for the viscous energy losses and velocity non-uniformity) and the pump efficiency (accounting for similar losses incurred in the pump):

$$\eta_0 = \eta_I \eta_{duct} \eta_P \tag{3.12}$$

Let us first have a look at the ideal efficiency, which comes forth from the often called jet efficiency or momentum efficiency for a waterjet system in free stream conditions (see e.g. Etter et al. (1980):

$$\eta_{jet} = \frac{P_{TE}}{P_{JSE}} \tag{3.13}$$

This jet efficiency accounts for the axial kinetic energy losses in the conversion from hydraulic power P_{JSE} to thrust power P_{TE}. This efficiency is analogous to the ideal efficiency used in propeller hydrodynamics. When for waterjets, the free stream condition is defined as the condition with the nozzle centreline situated at the free surface, ambient pressure at the nozzle and undisturbed flow in the intake, Eq. 3.13 transforms into:

$$\eta_I = \frac{2}{1+NVR} \tag{3.14}$$

where,
NVR = nozzle velocity ratio;
$NVR = \overline{u_6}/U_0$, or

$$\eta_I = \frac{4}{3+\sqrt{1+2C_{TN}}} \tag{3.15}$$

where,
C_{TN} = thrust loading coefficient;
$C_{TN} = T_{net}/\left(\frac{1}{2}\rho U_0^2 A_N\right)$

Interaction Terms. The major advantage of the introduction of separate interaction terms is that they refer directly to the physical process that is responsible for the energy loss or gain incurred.

Interaction on Momentum. The flow ingested by the jet is distorted by the hull. This distortion can be separated into a potential flow distortion (different pressure or velocity field outside the boundary layer) and a viscous flow distortion (contained within the boundary layer). There has been much debate on the correctness of a pressure term in the ingested momentum, to derive the net thrust produced by the waterjet. It was demonstrated by van Terwisga and Alexander (1995), however, that such a pressure should not occur in the relation for the net thrust, although the pressure contribution should initially be included in the momentum balance for the control volume.

Applying only the viscous momentum deficit for the ingested momentum in operational conditions, then leads to the following simple form for the momentum interaction efficiency:

$$\frac{1}{\eta_{mI}} = 1 + \frac{1-c_{m1}}{NVR-1} \tag{3.16}$$

where
c_{m1} = momentum velocity coefficient due to the viscous boundary layer velocity distribution at station 1 (equivalent to β_{m1} in Scherer et al. (2001)). See also ITTC Procedure 7.5-02-05-03.1

Interaction on Energy. The effect of the hull distorted flow on the energy balance of the waterjet is expressed in the energy interaction efficiency η_{eI} (Eq. 3.9).

The effective jet system power P_{JSEO} in the free stream condition as defined in the section on the waterjet system can be simplified into:

$$P_{JSE0} = \tfrac{1}{2}\rho Q\left(\overline{u}_{exn}^{2} - U_0^2\right) \tag{3.17}$$

In operational conditions, the effective jet system power can obtained from:

$$P_{JSE} = E_7 - E_1 \tag{3.18}$$

Scherer et al. (2001) extensively elaborate on the contributions in the energy fluxes. These relations are useful when detailed velocity and pressure measurements are available. The relations may be substantially simplified if it is assumed that the velocity distribution in the nozzle flow is effectively uniform and free of swirl and the pressure in the nozzle is equal to the ambient pressure (parallel outflow). A further simplification can be obtained when it is assumed that the boundary layer at the intake is thin, i.e. the pressure gradient rectangular to the hull is negligible throughout the boundary layer.

This condition is generally fulfilled for high speed hull forms with flat buttocks in the aft-body. In this situation, Eq. 3.9 can be rewritten into:

$$\frac{1}{\eta_{eI}} = 1 - \frac{gz_6}{\frac{1}{2}U_0^2\left(NVR^2 - 1\right)} + \frac{\left(1-c_{e1}^2\right)\left(1-C_{p1}\right)}{\left(NVR^2 - 1\right)} \quad (3.19)$$

where,

c_{e1} = energy velocity coefficient due to the viscous boundary layer velocity distribution at station 1 (equivalent to $\sqrt{\beta_{e1}}$ in Scherer et al. (2001)). See also ITTC Procedure 7.5-02-05-03.1

The second term on the right-hand side of Eq. 3.19 may be regarded as a typical potential flow effect in the interaction efficiency, which is caused by the change in elevation of the nozzle. This term may also be written as the ratio between the nozzle elevation above the still waterline z_n and the required pump head in free stream conditions H_0, expressed in meters water column mwc: z_6/H_0.

The third term on the right-hand side represents viscous energy losses in the ingested flow, caused by the friction of the stream-tube along the hull. If no boundary layer is present (uniform flow, $c_{e1}^2 = 1$), this term vanishes. In a retarded potential flow, where the pressure coefficient C_{p1} is increased, the effect of the viscous energy losses in the boundary layer is diminished. This can be understood if one recalls that the frictional energy losses are contained in the kinetic energy in the boundary layer. If all energy would be stored in potential pressure energy (such as e.g. in the stagnation point), there would be no viscous losses.

Interaction on Thrust and Drag. As opposed to propeller theory, the thrust deduction of a waterjet is more than a factor accounting for the different hull resistance due to the propulsor action. Although this effect is still the most dominant contribution to the thrust deduction for waterjets, another contribution occurs, being the difference between the change in momentum flux ΔM and the net thrust acting on the hull. The relation between the two quantities is discussed in Section 3.3.

Here we will only note that this *latter* contribution to the thrust deduction becomes only noticeable for the situation where the transom and nozzle opening are not yet fully ventilated. In this situation, the difference between the two quantities may contribute to the thrust deduction in a similar order of magnitude as the different hull drag does. This was concluded from an attempt to assess the different contributions from a systematic and theoretical point of view (Van Terwisga, 1996). In all other situations, the thrust deduction represents essentially the resistance increment of the hull due to the jet action.

3.3 Governing Equations

Relations for the delivered thrust and corresponding required power will be derived from the conservation laws of momentum and energy respectively. For this derivation, we will consider the conservation laws in their integral form. A body-fixed Cartesian coordinate system is used, with the x-ordinate oriented parallel to the local buttock (parallel to AD) and the z-ordinate pointing downward. For reasons of simplicity, it is assumed here that the jet, discharged from the nozzle (station 6) is oriented parallel to the x-ordinate.

Tensor notation is used throughout the equations with the Cartesian summation convention. In any product of terms, a repeated suffix is held to be summed over its three values 1, 2 or 3 (or x, y and z). A suffix not repeated in any product can take any of the values 1, 2 or 3.

Thrust. According to Newton's second law, "the change in momentum flux over a given control volume equals the sum of the forces acting on that control volume". This law

is used to derive an expression for the net thrust that is available to propel the hull.

The reaction force pertinent to this change in momentum is in equilibrium situations approximately equal to the net thrust acting on the hull, as will be shown in the following. Care is needed, however, to derive the net thrust from the change in momentum flux, because there are a number of surface integrals included in the momentum equation, that do not represent forces acting on the hull. The conservation law of momentum yields the following equation for a steady situation in i-direction in its integral form:

$$\iint_{A_1+A_6} \rho u_i \left(u_k n_k\right) dA = \iint_{A_1+A_2+A_3+A_6} \sigma_i dA + \iiint_{V_{3-5}} \rho F_{pi} dV + \iiint_{V_{1-6}} \rho F_i dV \tag{3.20}$$

where,

$$\iint_A \sigma_i dA = \iint_A \sigma_{ij} n_j dA$$

and σ_{ij} = total mean stress; $-p\delta_{ij} + \tau_{ij}$

p = time averaged pressure

δ_{ij} = Kronecker delta (equal to 1 if i=j and 0 otherwise)

τ_{ij} = total shear stress tensor; $\tau_{ij}' + \tau_{ij}''$

τ_{ij}' = viscous stress; $2\mu S_{ij}$

μ = dynamic viscosity of fluid

S_{ij} = time averaged rate of strain

τ_{ij}'' = contribution of turbulent motion to the stress tensor; Reynolds stress tensor

The term on the left-hand side represents the change in momentum flux $\Delta\overline{M}_i$ in i-direction. The terms on the right-hand side represent the forces acting on the control volume. The first term represents the pressure and tangential stress force acting on the boundaries of the Control Volume of the waterjet defined between stations 1 and 6. The second and the third term represent the volume forces of the pump and the gravity force component in i-direction respectively.

A net thrust $\overline{T}_{net}$ can now be defined as "the force vector acting upon the material boundaries of the waterjet system (A_3+A_4) and the pump volume $V_{3\text{-}5}$, directly passing the force through to the hull".

We will consider the component of the net thrust in x-direction T_{netx}, which will be abbreviated to T_{net} in the following. In tensor notation, the equation for the net thrust then reads:

$$T_{net} = -\iint_{A_3+A_4} \sigma_x dA - \iiint_{V_P} \rho F_{px} dV \tag{3.21}$$

The minus sign in the right-hand term occurs because of the orientation of the normal vectors, pointing out of the flow or control volumes.

The thrust deduction fraction t as defined by Eq. 3.6 can now be interpreted as the change in hull resistance due to the jet action. A fraction t_2 can additionally be introduced to allow for the discrepancy in the net thrust T_{net} and the change in momentum flux $\Delta\overline{M}_x$:

$$\Delta\overline{M}_x (1 - t_2) = T_{net} \tag{3.22}$$

Substitution of Eqs. 3.20 and 3.21 provides us with an expression for the discrepancy t_2 in terms of the forces acting on the stream-tube model:

$$t_2 = \frac{1}{\Delta\overline{M}_x} \left\{ \iint_{A_1+A_2} \sigma_x dA + \iint_{A_6} \left(\sigma_x - \sigma_{x0}\right) dA - \iint_{A_4} \sigma_x dA + \iiint_{V_{1-6}} \rho g_x dV \right\} \tag{3.23}$$

Generally, when the nozzle is fully ventilated or the nozzle and its projection on the stern are fully submerged, this contribution to the thrust deduction is negligibly small according to van Terwisga (1996). Significant values for t_2 have been found, however, in model experiments at the ship speed where the transom stern was clearing.

Power. Analogous to the derivation of the thrust equation, the equation for the required power is derived from the conservation law of energy.

The conservation law of energy in words reads that "the rate of change of the total energy per unit time for a certain amount of mass, equals the sum of the work per unit time, done by the forces acting on the surface, and the amount of external energy that is supplied per unit time". This latter contribution represents the power delivered to the pump impeller P_D.

The total energy per unit mass can be written as:

$$e = e_{kin} + e_{pot} + e_{\text{int}} \tag{3.24}$$

where,
e_{kin} = kinetic energy; $\frac{1}{2}u^2$
e_{pot} = potential energy
e_{int} = internal energy

The conservation of energy equation can now be written in the following integral form:

$$\iint_{A_1+A_6} \rho\left(\tfrac{1}{2}\mathbf{u}^2 - g_j x_j\right) u_i n_i dA + \psi_{diss} = \iint_{A_1+A_2+A_6} \left(-p u_i n_i + u_i \tau_{ij} n_j\right) dA + P_D \tag{3.25}$$

Because transport of mass only occurs through the areas A_1 and A_6, only these areas contribute to the transport of kinetic and potential energy through the volume boundaries. The rate of change of internal energy for an incompressible fluid can be written as:

$$\psi_{diss} = \iiint \frac{1}{\rho} \tau_{ij} \partial_j u_i dV \tag{3.26}$$

This term represents the viscous energy losses within the flow, which are converted into heat.

The contribution of the work done by surface forces, acting on the boundaries of the control volume is represented by the first term on the right-hand side of Eq. 3.25. No work is done by the surface tension forces within the ducting of the waterjet, due to the non-slip condition at the corresponding surfaces. A similar observation can be made for the pressure forces acting perpendicular to the dividing stream surface.

It is furthermore assumed that there is no exchange of heat through the volume boundaries. The external rate of change of energy that is supplied to the system is therefore solely due to the pump delivered power P_D.

3.4 Determination of Flow Rate, Momentum and Energy Fluxes

There are basically two ways to determine the required flow rate, momentum and energy fluxes from experiments. One way is to perform flow rate calibration tests, and to relate the flow rate to a suitable measurement signal in the waterjet. The other, and as will appear the better way, is to perform a bollard pull test and measure the jet thrust directly from a force transducer. This force, designated jet thrust T_{Jx}, can then similarly be related to a suitable measurement signal in the waterjet.

Performance considerations should play a dominant role in the selection of the most suitable procedure, apart from economic considerations. To this end, we will use uncertainty in net thrust as a performance indicator. The model thrust is a suitable performance indicator, as this variable plays a dominant role in the extrapolation procedure and hence in the final power-speed prediction. Consequently, both the precision and bias errors, as well as their propagation into the uncertainty of the net thrust should play a role in the selection of the calibration procedure.

The model net thrust can thus be obtained from the change in momentum flux (see Eq. 3.22) from flow rate measurements:

$$\Delta\overline{M}_x = \frac{\rho Q_J^2}{A_N}\cos\theta_N - \rho Q_J c_{m1} U_0 \qquad (3.27)$$

or from jet thrust measurements:

$$\Delta\overline{M}_x = T_{Jx} - c_{m1} U_0 \sqrt{\frac{T_{Jx}\rho A_N}{\cos\theta_N}} \qquad (3.28)$$

In a similar way, relations for the effective jet system power P_{JSE} can be derived as a function of either flow rate or jet thrust.

In the substitution of flow rate for jet thrust, it is assumed that the jet velocity profile upon discharge is sufficiently uniform to equate the mean momentum and energy velocities to the mean volumetric velocity (see also Section 4.3 on Jet Velocity Survey). Should this not be the case, the differences in mean velocities can be accounted for with momentum and energy velocity coefficients (c_m and c_e or β_m and β_e), as introduced in Section 3.2. The relation between jet thrust and flow rate is then given by:

$$T_{jet} = \frac{\rho Q_J^2}{A_N} c_{m6} \qquad (3.29)$$

where,
c_{m6} = momentum velocity coefficient.

Apart from the uncertainty in flow rate and jet thrust measurement itself, the sensitivity of the net thrust for variations in either flow rate or jet thrust also contributes significantly to the overall uncertainty. The relative sensitivities θ' can be calculated from:

$$\theta'_{x_i}\left(T_{net}\right) = \frac{\partial T_{net}}{\partial x_i}\frac{\overline{x_i}}{\overline{T}_{net}} \qquad (3.30)$$

where,
x_i = any parameter in the relation for T_{net} and over-bars denote average values.

Starting from the Eqs. 3.27 and 3.28, the relative sensitivities θ'_i can now be expressed as functions of the nozzle velocity ratio NVR and the momentum velocity coefficient in the intake c_{m1}.

The relative sensitivity for an error in the flow rate θ'_{QJ} can directly be compared to the relative sensitivity for an error in the jet thrust θ'_{TJx}. This is done in Fig. 3.3a for a representative value of $c_{m1} = 0.9$. This graph shows that the jet thrust procedure shows a sensitivity that is half the sensitivity of the flow rate procedure over the complete NVR range.

A similar comparison on the relative sensitivity of net thrust can be made for the error contributions by the nozzle area A_N and the specific mass of water ρ. The sensitivity for A_N is plotted in Fig. 3.3b for both calibration procedures. It shows that the difference between thrust calibration and flow rate calibration is here considerable in the NVR region of practical interest (roughly for $1.5<NVR<3$). With regard to the uncertainty in nozzle area A_N, it is noted that the tolerance in the nozzle diameter manufacture is about 0.05 to 0.1 mm. An additional error may, however, be introduced by a possible vena contracta (Station 7) behind the nozzle discharge area (Station 6), which is usually unknown and therefore discarded.

A comparison on the relative sensitivity of net thrust for errors in specific mass is given in Fig. 3.3c. Again, the thrust calibration procedure shows the lower sensitivity in the practical NVR range. As regards the uncertainty in specific mass, it is noted that during a number of flow rate calibration tests air bubbles were observed in the water discharge. This air content could have affected the specific mass within the waterjet. It is therefore concluded that the error due to deviations in the specific mass in the flow rate calibration procedure is

higher than it is in the thrust calibration procedure.

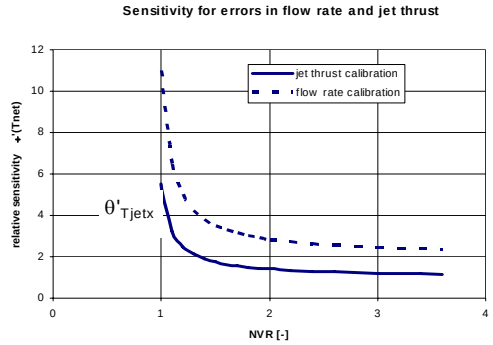

a

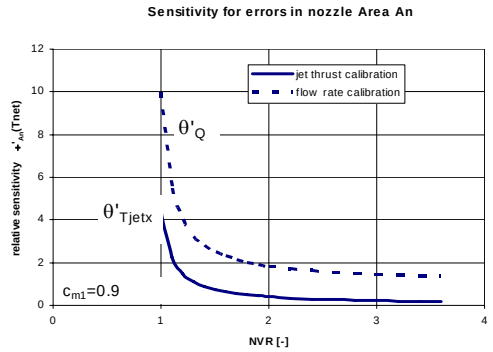

b

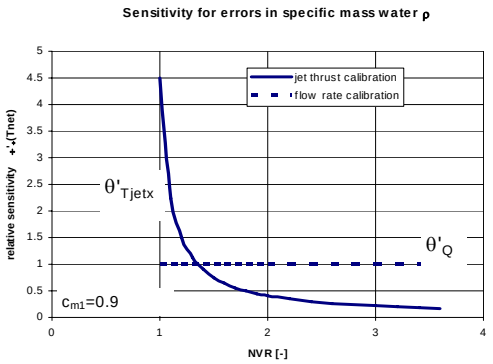

c

Figure 3.3- Relative sensitivities for jet thrust and flow rate calibration, for nozzle Area A_N and for mass density ρ.

3.5 Data Reduction and Scaling

Data Reduction. The global flow through the whole data acquisition and the data reduction phase is presented in Fig. 3.4. The four horizontal blocks indicate the four main processes from which the data are collected.

The first process contains the derivation of relevant data from the model or ship geometry. Essentially the nozzle discharge diameter (D_N) or the nozzle discharge area (A_N) is required, together with an estimate of the width of the capture area at station 1. These dimensions largely determine the momentum and energy fluxes through the respective stations for a given flow rate Q. Apart from the intake geometry data, the length of the hull and the wetted surface of the hull are required for an estimate of the tow force F_D that is to be applied during the propulsion tests.

Subsequently, a resistance test and a wake-field measurement on the model in resistance test configuration (that is closed intake and nozzle, same weight and centre of gravity as with working jets) is conducted. The resistance test, although not strictly necessary, is recommended because it provides a valuable check of the validity of the propulsion test through evaluation of the thrust deduction fraction *t*.

The wake-field measurement is to be conducted with closed intakes (nominal wake-field), in order to be free of intake induced velocities. The boundary layer velocity profile is used as a measure for the distortion of the inflow in the capture area 1A, caused by the hull, as can be seen from Fig. 3.1 and Eqs. 3.7 and 3.9. Based on the very definition of the momentum and the energy interaction coefficient, only the hull effect on the flow should be incorporated in the ingested boundary layer. This distortion on the inflow is then superimposed on the inflow in the waterjet in free stream conditions (comparable with the nominal wake-field of propellers). In this way, the interaction effect of the hull on the jet can be quantified.

In determining the hull distorted velocity profile, one should take care that the suction from the waterjet intake is not included, as this suction effect is also present in free stream conditions, once one is sufficiently close to the waterjet. The intake induced flow is thus accounted for in the jet system characteristics.

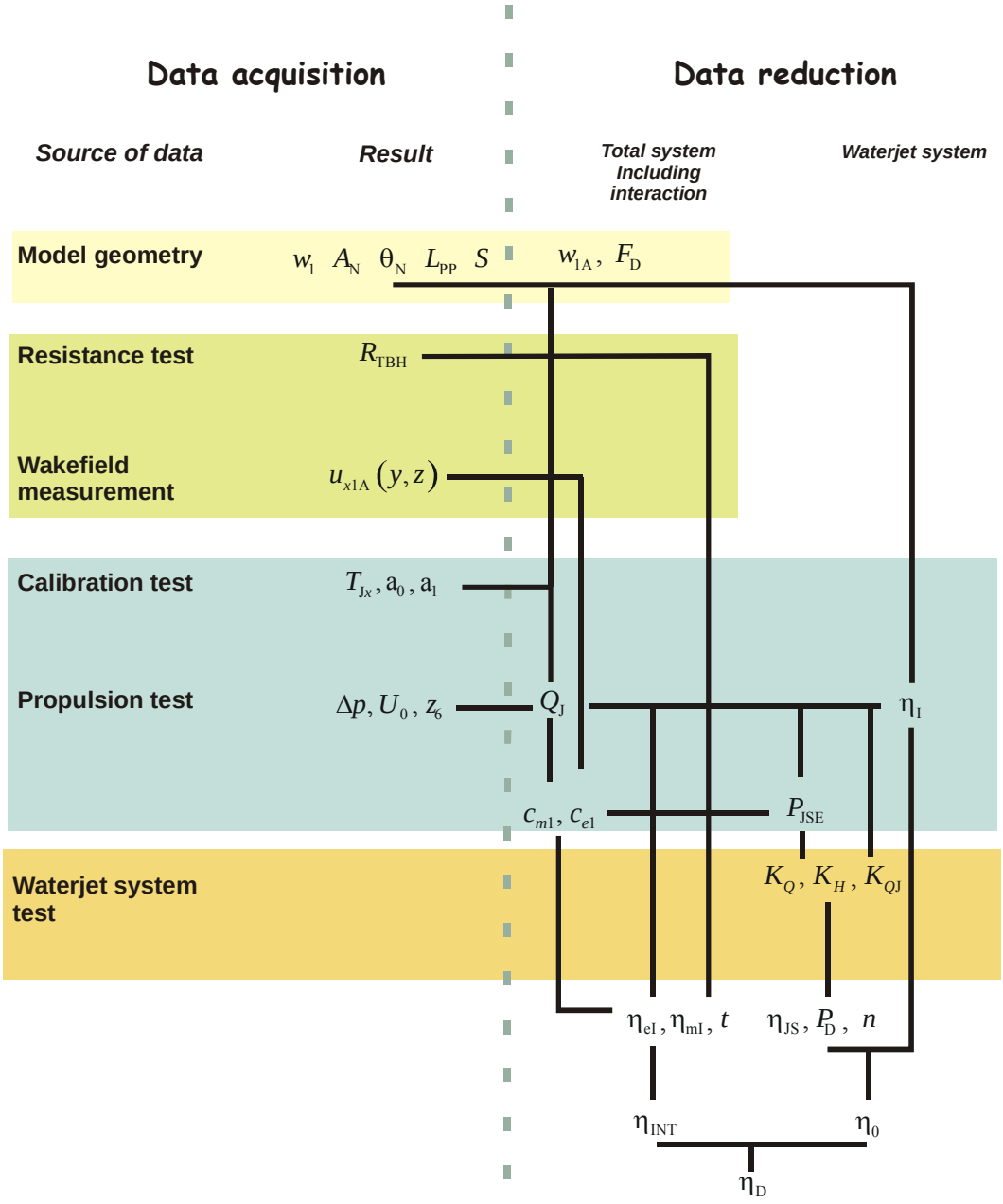

Figure 3.4- Data flow through data acquisition and data reduction phase for determination of powering characteristics from model tests.

A true interaction effect would also include the effect of the waterjet suction on the hull distorted flow (similar to the effective wake-field on a propeller). However, this latter component is generally small for straight afterbodies as normally designed for waterjet propulsion.

The third process consists of a calibration test and the actual propulsion test. The calibration test is needed to obtain a reliable relation between the transducer signal and the flow rate through the waterjet system. Often differential pressure transducers will be used to measure the flow rate. Based on the experience gained from the standardization tests, it is proposed that the flow rate is derived from jet thrust measurements during bollard pull, for a variety of impeller revolution rates.

Flow rate calibration through a force measurement (measuring momentum flux) is preferred over direct flow rate measurement (e.g. through a flow meter), as is argued in Section 3.4.

Once the flow rate, wake-field and nozzle sinkage have been measured for the required operating condition, the data necessary for the determination of Jet System Power, P_{JSE} including waterjet-hull interaction effects are available.

It appeared from the standardization tests that there are a lot of different interpretations in the choice of the correct operating condition (defined by tow force F_D). There are, however, only two different philosophies which lead to justifiable operating conditions: Thrust identity or flow rate identity. The first philosophy is the current standard and sets the non-dimensional thrust equal for both model and ship. The philosophy assumes that when the model thrust coefficient is equal to the full scale equivalent, the derived thrust deduction fraction is the same for both model and full scale.

This assumption, however, only makes sense when the pressure and shear stress distribution about the aft body (responsible for the thrust deduction fraction) strongly depend on the thrust vector. In the case of waterjet propulsion, however, the pressure and shear stress distribution about the aft body are primarily determined by the ingested flow rate. If thrust identity is used now to determine the ship's self-propulsion point, relatively too little flow rate is ingested because of the relatively thicker boundary layer at model scale (see also Wilson et al., 2003 and Van Terwisga et al., 2002).

Therefore, flow rate identity may be a better philosophy to determine the model operating condition. The tow force can then be found from the relation between thrust (or change in momentum flux) and flow rate (Eq. 3.27). In its non-dimensional form, this equation reads:

$$C_{TN} = 2NVR\left(NVR - c_{m1}\right) \tag{3.31}$$

It is assumed in this derivation that the jet discharge is horizontal ($\theta_N = 0$). This equation can now be used to determine the non-dimensional flow rate NVR_m in case of thrust identity ($C_{TN\text{-}m} = C_{TN\text{-}s}$) or the model thrust coefficient $C_{TN\text{-}m}$ for flow rate identity ($NVR_m = NVR_s$). Once the working point on model scale has been established, the thrust deduction fraction *t* can be determined from the experiment. More details on the experimental procedure are provided by Scherer et al. (2001) and later by Wilson et al. (2005).

Although the flow rate identity philosophy appears to be a promising method, yielding slightly higher thrust deduction fractions, too little experience has been collected with this new method. The preferred method is therefore still based on thrust identity, applying a proper correction to scale the ingested boundary layer to full scale values. In this procedure, first the thrust requirement for full scale is determined (through the determination of the thrust deduction fraction *t*). From this thrust requirement and the estimated full scale boundary layer, the corresponding flow rate is computed. The scaling procedure to account for viscous scale effects and velocity non-uniformity effects in intake and nozzle flow is given in ITTC Procedure 7.5-02-05-03.1 and schematized in Fig. 3.4. Details on the effect of velocity non-uniformity can also be found in Scherer et al. (2001).

The results of the propulsion test will have to be fed into the jet system characteristics, however, to arrive at the power that needs to be delivered to the impeller and the corresponding impeller rotation rate. The determination of the jet system characteristics is depicted here as the fourth process. These jet characteristics are preferably determined on a larger jet model and can be determined on a circulating water tunnel (see Chapter 5).

Extrapolation. Extrapolation from model scale to full scale is required for the powering data representing the waterjet system, the hull and the mutual interaction. This Section addresses the extrapolation of waterjet-hull interaction data and briefly notes the extrapolation of waterjet system data. Extrapolation of the bare hull resistance is a daily task for model basins and is therefore not further elaborated here.

Waterjet-Hull Interaction. The recommended procedure for the determination of the interaction coefficients from the propulsion test, is based on thrust identity, as argued in the foregoing. With the relations for the interaction coefficients derived in the foregoing, scale effects in interaction data can be acknowledged and to a large extent accounted for. The procedure is schematized in Fig. 3.4. It uses the Froude scaling principle as a starting point and applies viscous corrections necessary on the viscous part of the bare hull resistance, and consequently on the boundary layer thickness and velocity profile within this layer.

Analogous to the proposal by the Savitsky et al. (1987), the hull thrust deduction fraction is considered free of scale effects. This assumption, made without justification by the 1987 ITTC, is justified here with reference to the hypothesis on the hull thrust deduction. When studying the definition of the thrust deduction fraction (or rather the resistance increment) it becomes clear that at least one term consists that is prone to viscous scale effects:

$$\iint_{A'D} \sigma_{x0} dA \tag{3.32}$$

This term represents the change in hull resistance due to the missing area projected in the hull plane. As this contribution is O(1%) of the bare hull resistance, and the scale effect on resistance, expressed in F_D is typically of O(10%) of the resistance, the viscous scale effect on the intake plane contribution is negligible.

The momentum interaction efficiency η_{mI} can be assessed from Eq. 3.16 and is seen to be a function of NVR and momentum velocity coefficient at station 1A, c_{m1}. For a given waterjet system, the nozzle velocity ratio depends on the flow rate Q and the ship speed U_0. The flow rate is governed by the thrust requirement, as expressed in Eq. 3.27. It is to a lesser extent affected by viscosity, which in turn depends on the flow rate and the boundary layer characteristics. Consequently, an iteration process is required to match flow rate, net thrust and momentum velocity coefficient.

The boundary layer characteristics in terms of thickness δ and velocity distribution $u(z)$ should be measured during a test with a closed intake (nominal intake field).

Alternatively, the boundary layer characteristics can be estimated from a semi-empirical formula. In the latter case, care should be taken that the uncertainty in the estimate does not dominate the overall uncertainty in the experiment (see also Procedure 7.5-02-05-03.3)

Extrapolation of the boundary layer characteristics is done through a Reynolds dependent relation for the thickness. The velocity profile is considered to follow the power law:

$$\frac{u(z)}{U} = \left(\frac{z}{\delta}\right)^{1/n} \qquad for\ z \le \delta \tag{3.33}$$

The power coefficient n for the model can be matched from the measured velocity profile in the imaginary intake.

A power value for n of approx. 9 for the full scale situation is suggested.

After the flow rate is solved from the above process, the energy velocity coefficient c_{e1} is readily available. The nozzle sinkage in the energy interaction term (Eq. 3.19) is considered free of scale effects and is therefore simply obtained from Froude scaling.

Waterjet System Characteristics. The full scale waterjet system data are required in the process of the powering performance prediction as illustrated in Fig. 3.4. They can be based on a combination of pump tests and intake analysis or on a waterjet system test. The results from the standardization tests on this type of testing is reported in Chapter 5. Scaling of the results is not treated further in this report.

4. RESULTS OF SELF-PROPULSION TESTS

4.1 Background

The main objective of self-propulsion tests with waterjets is to determine the flow rate and head that is to be delivered by the waterjet system. With this information, and the jet system characteristics, either obtained from the jet manufacturer or directly from model tests (see Chapter 5), the relation between delivered power P_D, ship speed and impeller rotation rate can be determined.

Contrary to screw propellers, waterjet systems are propulsion devices that are so much integrated with the hull that it is difficult to determine the propulsion interaction data such as wake fraction and thrust deduction. Model testing of marine vehicles with waterjet propulsion systems therefore presents problems which cannot be dealt with in exactly the same manner as in tests with propeller driven craft.

For a waterjet driven craft, the prediction of the prototype performance must be based on a valid theoretical model of overall system performance, based on element performance and a rigorous accounting method of all interaction effects.

As presented in Chapter 3, the ITTC efforts outline an experimental procedure that is able to assess performance data in a form suitable for expanding to full scale. This is done in combination with a method that permits the determination of total system performance from tests of the separate components.

Looking to the copious preceding literature, only in 1987 the High-Speed Marine Vehicle Committee defines the first guide lines. These concentrated on the techniques and procedures used for model tests involved in the design and the performance predictions for waterjet-propelled craft of the planning, semi-displacement, and SES types.

In 1996 the Waterjet Group of 21st ITTC presented a revised prediction method based upon momentum flux considerations where many elements were in line with the earlier ITTC proposal. There were, however, some differences, the most important being that the gross thrust concept as defined at the 18th ITTC (1987) was replaced by the change in momentum flux ΔM, balancing the thrust from the pump and the internal ducting force, plus the change of hull resistance caused by the action of the propulsion unit, including trim effect. The same Group proposed as an alternative to the momentum flux method the direct thrust measurement method.

In the following the first method was preferred but, because there was still serious debate over the details of the momentum flux method, the Specialist Committee on Waterjets of the 22nd ITTC was appointed to improve the understanding of waterjet hydromechanics and powering prediction methods.

The Committee established contacts with jet manufacturers having in mind that, when predicting the powering performance of a waterjet driven vessel, data from the jet manufacturer and from a towing tank should be matched. It is thereby important that flaws in the overall performance prediction due to misunderstandings are avoided. Consequently the Waterjet Committee planned a world-wide series of standardization experiments to assess the validity of the waterjet test procedures. Two additional experiments, the “waterjet

pump", and the "waterjet system" tests were proposed, supplementing the traditional self-propulsion test.

The report of the 22nd ITTC (Hoyt et al., 1999) describes the problem of waterjet powering prediction and gives details on the organization of the standardization exercise. The report of the 23rd ITTC (van Terwisga et al., 2002) gives an account of the progress and the outstanding issues in waterjet prediction. Despite the difficulties encountered in manufacturing and managing two different models travelling around the world at virtually no budget, the following institutions completed their own task: CEHIPAR, DTMB-NSWC, HMRI, INSEAN, KRISO, MARIN, and SVA.

A detailed presentation of data and discussion of results will be given in the following. Conclusions on the most reliable techniques for self-propulsion tests are derived.

4.2 Presentation of Data

At the time of this writing, there where nine participants in the self-propulsion experiments, of which only seven had provided data. These data sets are too large to provide in the body of this report, but they can be downloaded from the ITTC Waterjet Committee Web Site at www.ittc-wjc.insean.it.

The Committee had requested that predefined Excel datasheets be completed and returned to the Committee for analysis. This request was only partially met with a collection of free formatted Excel spreadsheets and partially complete standard forms received. The data found on the Web Site was transcribed into the format requested by the Committee as best as was possible.

The raw data in combination with the cross comparison and analysis found in this Report provides an initial look into the industry wide validity of a waterjet self-propulsion experiment. This analysis only scratches the surface. Due to the limited data submitted at speeds other than a Froude number of 0.60, and limitations in the size of this report, Froude number 0.60 will be the primary reference speed.

The down side of the double blind method employed was the inability to ask questions or request additional information from the participants. There were numerous numerical and typographical errors as well as missing information in the data received. The Committee corrected these data sets as best as could be done given the time and information available. It is hoped that the participating Organizations will review the results and then use this data to fine-tune their own procedures.

4.3 Discussion

The waterjet self-propulsion experiment was subdivided into six components from the point of view of data organization and analysis. These components dictated the datasheets that were to be used for reporting and analysis and are as follows:

- Bare Hull Resistance Tests
- Bare Hull Inlet Velocity Survey
- Working Inlet Velocity Survey
- Jet Velocity Survey
- Momentum Flux Calculations
- Full Scale Predictions

Bare Hull Resistance Tests. There were seven respondents to the bare hull resistance test of the 8.556 scale Athena model. The results for the bare hull with inlets covered is shown in Figs. 4.1 through 4.4.

The first issue to note is the lack of agreement in the test weight shown in the legend. The model was requested to be tested at the 264.17 tons (260 LT) load line. Although there should be some variation in model weight due to towing basin water temperature differences, the modelled displacement varied as much as 6.6% from the design displacement, as can be seen in Table A1 found in Appendix A.

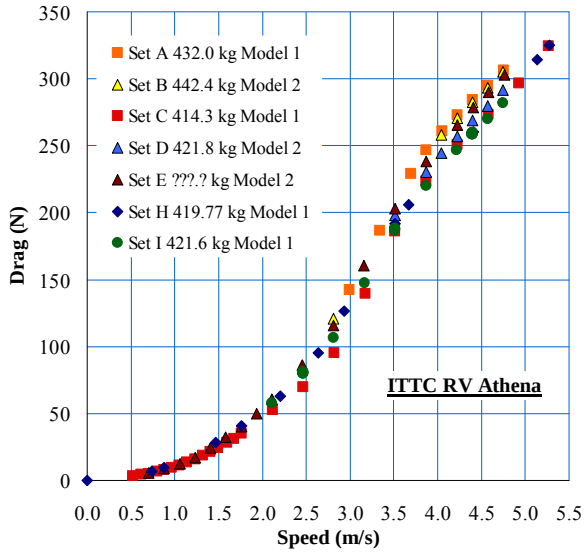

Figure 4.1- Comparison of measured model drag.

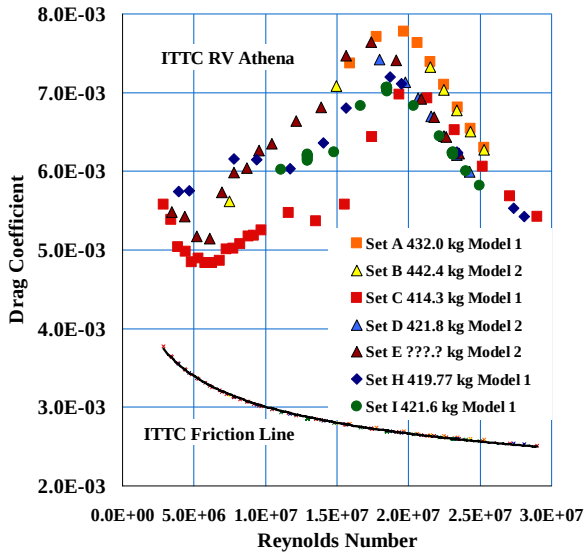

Figure 4.2- Comparison of computed model drag coefficients.

Theoretically, the dry test weight should have accounted for the fact that there was both some lost displacement due to the submerged portions of the inlet ducts as well as added weight due to the entrained water above the waterline. This should have given a target dry test weight of 261 tons. Instead of this target weight a dry test weight averaging around 273.6 tons was obtained. Assuming that every-one did attempt to ballast the model to the same load line, and assuming that there is no difference in hull geometry between the two models, then it must be assumed that the models were both built slightly oversize in volume by 4.8% with a scatter due to ballasting differences of 3.2%

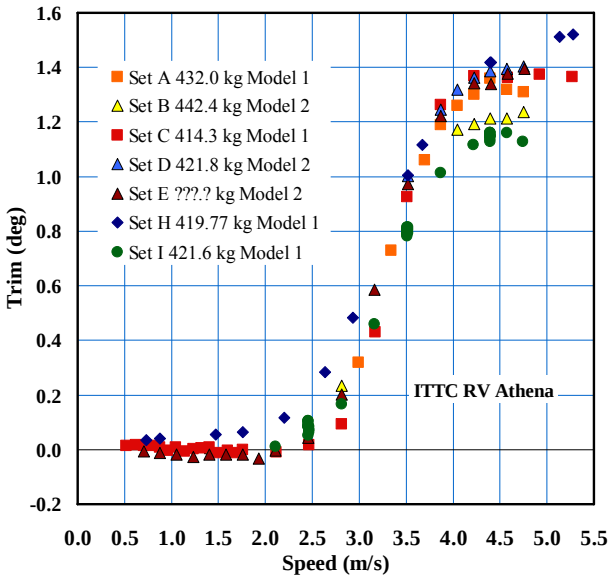

Figure 4.3- Comparison of measured model running trim.

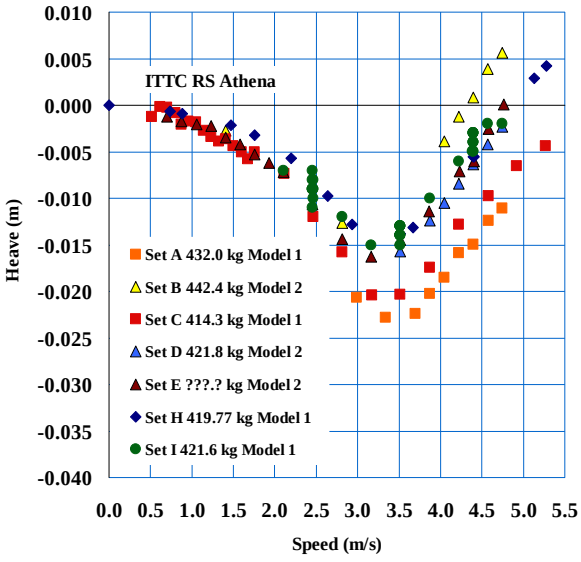

Figure 4.4- Comparison of measured model heave.

The next issue with the bare hull resistance data is the impression that there are two trend lines. Data sets A, B, and E seem to follow a trend line which is 7.0% higher than that followed by data sets C, D, H and I.

There is no correlation with which model was tested. However, Sets A and B, but not E were tested at a heavier displacement than the group. Overall there is a 4.5% scatter band in the resistance measurement.

However, this amount of scatter is greatly reduced to 1.0% for the higher group and 1.7% for the lower group. These differences do not seem to be due to the model that was tested, test displacement, or model age (degradation with time.)

One possible explanation could be the blockage, although this was only a 5.5 m long model, and the trim and heave data trends do not follow the drag results.

There appears to be considerable scatter in both the trim and heave results as can be seen in Table A1 found in Appendix A. Running trim has an overall scatter of 10.6% at a Froude Number of 0.60. This is reduced to 2.9% if the outliers are removed.

Heave looks even worse with an overall scatter of 117%, reduced to 55% with again the elimination of outliers.

It was hoped that differences between bare hull and powered attitude could be discerned. Given the small range measured, only 1.4 degrees for pitch and 15 mm for heave, there is a potential resolution problem. There also appears to be a problem with both determination of the fore and aft measurement points as well as consistent zeros. Stepping away from the numbers, and looking at the quantities it appears that the running trim was measurable to within 0.3 degrees and heave to within 16 mm.

Bare Hull Inlet Velocity Survey. Although the boundary layer in front of the intake should be measured with closed intakes, see Section 3.5, the Committee is aware that some institutes apply a procedure with an open intake. To investigate the effects of an open intake, the results for both closed and open intakes were requested.

In order to use the momentum flux method, information about the flow into the inlet duct is required. There still remains the debate whether the flow into a working or bare hull with closed inlets is the correct approach. There is also always concern there will be a loss in accuracy if a single measure of the boundary layer near the inlet centreline is used versus a comprehensive survey. It was hoped that a measure of the asymmetry in the flow would be obtained from these experiments.

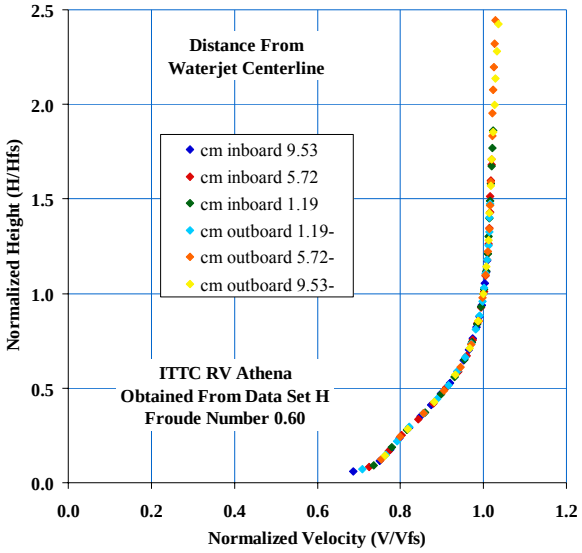

Figure 4.5- Boundary layer profile measured at station 1A with closed intake.

Based upon the data survey obtained from Data Set H, shown in Fig.4.5, it appears that the transverse uniformity in the flow when normalized is very good.

At least for the Athena, a single formulation for the boundary layer profile measured one pump diameter forward of the inlet tangency point can be used. A single measurement may be sufficient to determine the profile, however, it should be noted that although the profiles seem the same when normalized, the boundary layer thickness may vary transversely.

The bare hull velocity profiles reported were measured in a variety of ways. Both pressure and Laser Doppler methods were used. In the case of the pressure measurements both 5-hole and Pitot-static probes were employed.

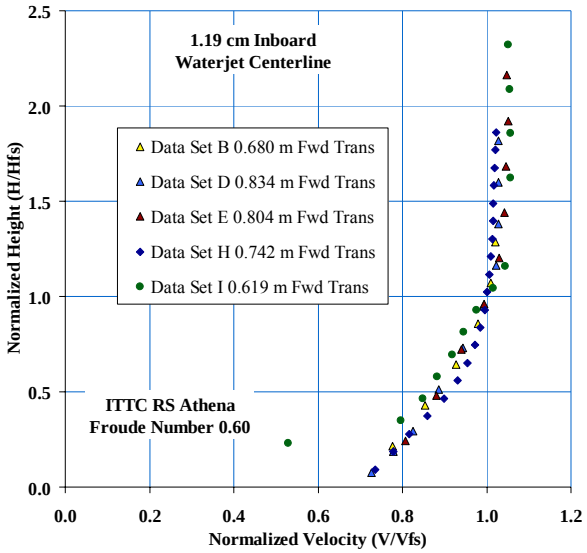

Figure 4.6- Comparison of boundary layer profiles at 1.19 cm inboard waterjet centreline with closed intake.

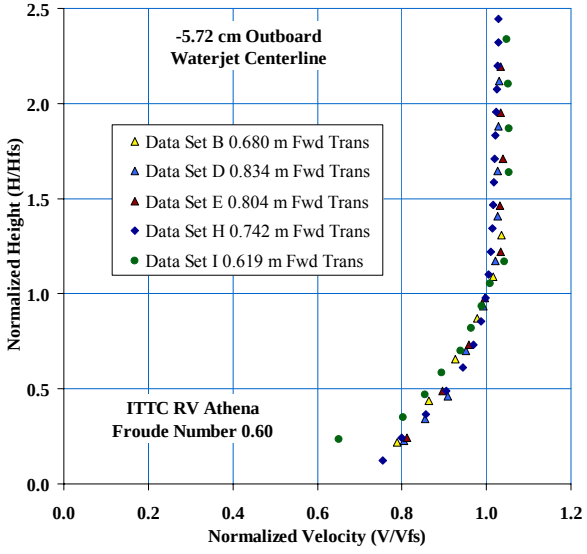

Figure 4.7- Comparison of boundary layer profiles at -5.72 cm outboard waterjet centreline with closed intake.

The agreement in the shape of the normalized velocity profile is good, as shown in the representative sets of data measured near Station 1 (Figs. 4.6 and 4.7). It should be noted that there are differences in the longitudinal location of the measurement plane, but even given this, the correlation is still good.

These measured profiles are used to determine the average velocity ingested past this measurement station as well as the 2nd and 3rd order velocity terms required to estimate thrust and power. Profile shape will affect these values.

Table 4.1- Effect of velocity profile on capture area and ingested fluxes with closed intake.

Cycloid shape	A Profile Full	H Profile Full	H Profile Uniform
Flow Rate (m^3/sec)	0.0378	0.0378	0.0378
Capture Height (cm)	6.60	6.62	6.64
Capture Width (cm)	20.73	20.81	20.86
Capture Area (cm^2)	102.60	103.39	103.87
Avg. Velocity (m/sec)	3.69	3.66	3.64
Momentum Vel. (m/sec)	3.77	3.75	3.73
Energy Velocity (m/sec)	3.82	3.79	3.78
cm (-)	0.858	0.851	0.847
ce (-)	0.869	0.862	0.858

To test the sensitivity of the velocity terms relative to profile shape at the capture area, 3 cases are compared in Table 4.1. Using Data Sets A and H, differences in measured profiles are compared. It appears that the shape change going from Data Set A to H will increase the average velocity by 0.54%, the momentum velocity by 0.45% and the energy velocity by 0.3%.

The sensitivity to transverse variation in the boundary layer thickness is shown in the comparison of the full Data Set H to a uniform field using the average of the two near centreline measurements. In this case it appears that the shape change going from the full Data Set H to a uniform H will decrease the momentum and energy velocity coefficients c_m and c_e with approx. 0.5%. The impact of these errors in measurement on thrust and power assessment is negligible, as demonstrated in ITTC Procedure 7.5-02-05-03.3 (Uncertainty analysis - Example for propulsion test).

Working Inlet Velocity Survey. Data for the survey of the inlet in-flow near Station 1A, while the model was near the self-propulsion point, was submitted by a few participants. Based upon the data survey obtained again from Data Set H, shown in Fig. 4.8, it appears that the transverse uniformity in the normalized velocity is also very good.

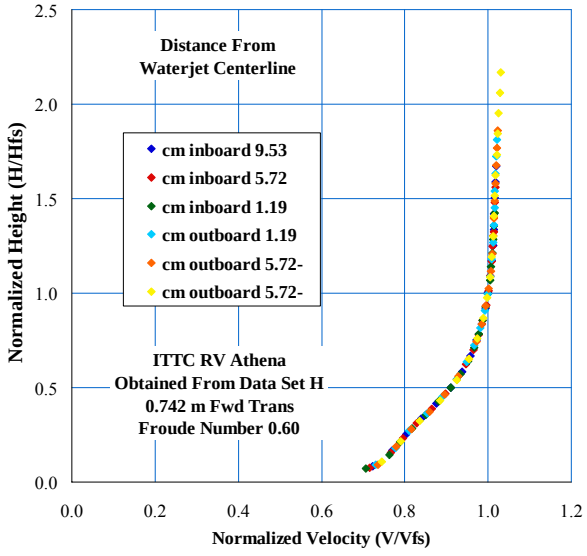

Figure 4.8- Boundary layer profile measured at station 1A for working jet with open intake near self-propulsion point.

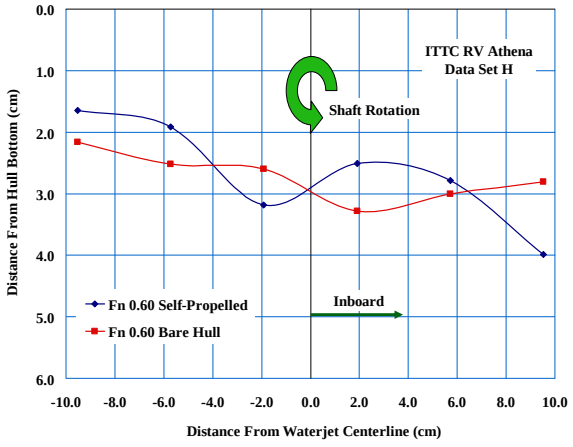

Figure 4.9- Height of 90% free stream velocity at station 1A for Fn = 0.60.

As a consequence, a single formulation for the boundary layer profile measured one pump diameter forward of the inlet tangency point can be used in the case of a working inlet.

The transverse variation in the boundary layer velocity profile, as well as a comparison between the bare hull and a working waterjet inlet is shown in Fig. 4.9. There appears to be a trend for the boundary layer to get thinner in the outboard direction.

Table 4.2- Effect of velocity profile on capture area and ingested fluxes with working intake.

	H Profile Bare Hull	**H Profile Working**
Flow Rate (m^3/sec)	0.0378	0.0378
Capture Height (cm)	6.62	6.59
Capture Width (cm)	20.81	20.72
Capture Area (cm^2)	103.39	102.45
Avg. Velocity (m/sec)	3.66	3.70
Momentum Vel. (m/sec)	3.75	3.78
Energy Velocity (m/sec)	3.79	3.83
cm (-)	0.851	0.860
ce (-)	0.862	0.870

There is also a pronounced effect caused by the operating waterjet inlet system shown in 4.9. One pump diameter forward of the inlet point of tangency there is a curl in the iso-surface defining 90% free stream. It appears that this surface is raised up towards the hull on the upward swinging side of the shaft, while being depressed on the downward turning side.

The effects of this shape change upon the velocity parameters are shown in Table 4.2. It appears that the shape change going from the bare hull to a working inlet for Data Set H will increase the average velocity by 0.97%, the momentum velocity by 0.99% and the energy velocity by 1.00%.

The agreement in the shape of the normalized velocity profile is not good in the case of the working inlet as can be seen in the representative sets of data measured near Station 1 shown in Figs. 4.10 and 4.11. Here the differences in the longitudinal location of the meas-

urement plane are having an observable effect. Data sets B and I being the closest to the inlet opening have seemed to lost the "no-slip" near the hull and have a larger over-speed in the free stream, all effects that would be expected near a working inlet.

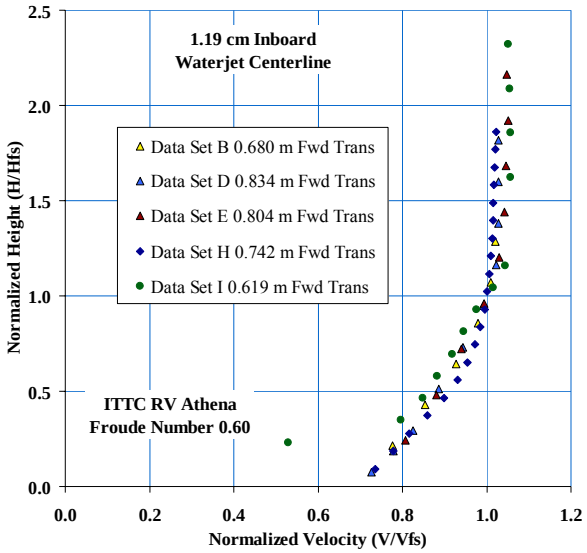

Figure 4.10- Comparison of boundary layer profiles at 1.19 cm inboard waterjet centreline for working jet with open intake near self-propulsion point.

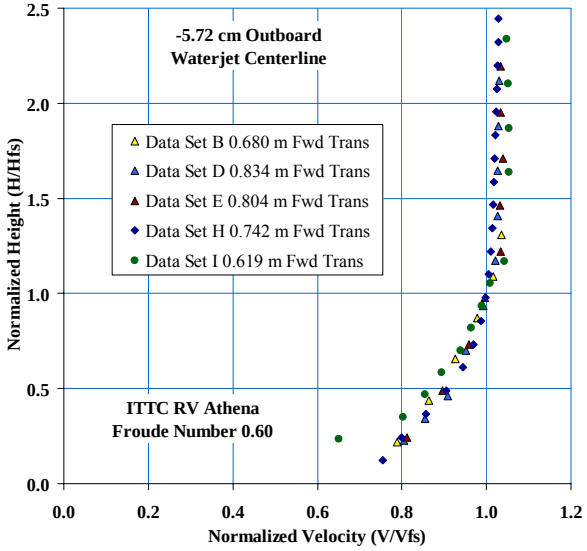

Figure 4.11- Comparison of boundary layer profiles at 5.72 cm outboard waterjet centreline for working jet with open intake near self-propulsion point.

Jet Velocity Survey. In order to use the momentum flux method information is needed about the velocity uniformity of the jet exiting the nozzle. There were six respondents who provided data of the jet velocity survey. The jet survey was measured with Laser Doppler, Pitot-static and 5-hole probes.

The jet survey cannot be integrated to estimate the flow rate accurately enough for the momentum flux method due to the error in measuring the velocities near the jet boundaries. It was determined that using the measured bollard thrust to calculate flow rate along with a multi-port velocity reference probe in the jet resulted in the lowest overall uncertainty for the flow rate measurement. A multi-port probe is strongly recommended to account for changes in the velocity distribution with forward speed.

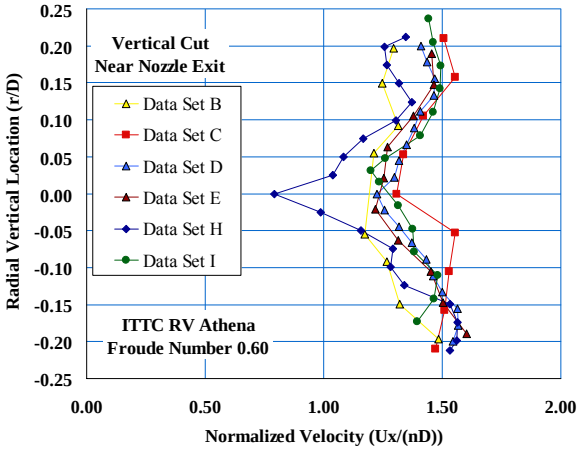

Figure 4.12- Vertical jet velocity profiles measured at station 6 for a jet operating near self-propulsion point.

The jet velocity surveys from the six respondents for a Froude Number of 0.6 varied in RPM, and both radial and angular position. The vertical and horizontal positions were taken in all the jet surveys for the axial velocity component and this data was chosen to show the velocity comparisons. Since the speeds were different for the six respondents, the axial velocities were normalized by the rotational speed and pump diameter and the radius was

normalized by pump diameter as shown in Figs. 4.12 and 4.13.

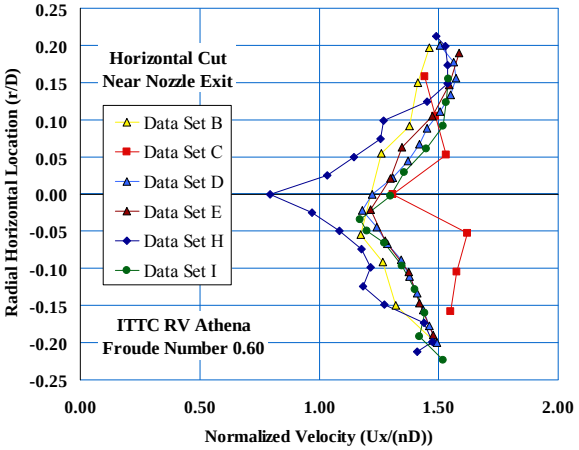

Figure 4.13- Horizontal jet velocity profiles measured at station 6 for a jet operating near self-propulsion point.

The maximum deviation from the mean, ignoring Data Set H since it was taken upstream of the nozzle, is 3.8% on the normalized axial velocity. The average momentum non-uniformity factor, c_{m7} is 1.004, and the average axial energy non-uniformity factor c_{ex7} is 1.005 and the average total energy non-uniformity factor c_{e7} is 1.01.

Momentum Flux Calculations. The importance of a proper flow rate measurement, either directly measured or through jet thrust measurement, has already been addressed in Section 3.4. Unfortunately few of the responders elected to perform experiments at speeds other than a Froude number of 0.6, and as a result most of the flow rate data are clustered around this point.

Figure 4.14 shows the relation between flow rate and waterjet impeller speed. For dataset H, it is known that the flow rates were derived from a bollard pull calibration test and from a laser survey underway. In this case, agreement between integration of the measured velocity field within the duct, and the determination of apparent flow rate from the bollard thrust (Eq. 3.29) is very good.

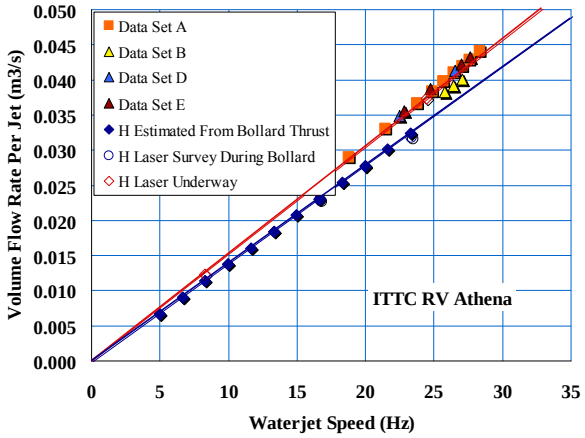

Figure 4.14- Derived relations for flow rate as a function of impeller speed.

Figure 4.14 also clearly shows that the relationship between waterjet impeller speed and flow rate is also effected by advance speed. With increasing advance speed, the waterjet system unloads and will produce a higher flow rate, making the impeller rate as a single measure for flow rate unsuitable. Methods to overcome this problem have been discussed in Section 3.4. It appears that the unknown methods used for data sets A, B, D and E to determine flow rate when underway, are following the same trend line. The underway trend line yields higher flow rates than the bollard measurement for a given impeller speed, as would be expected.

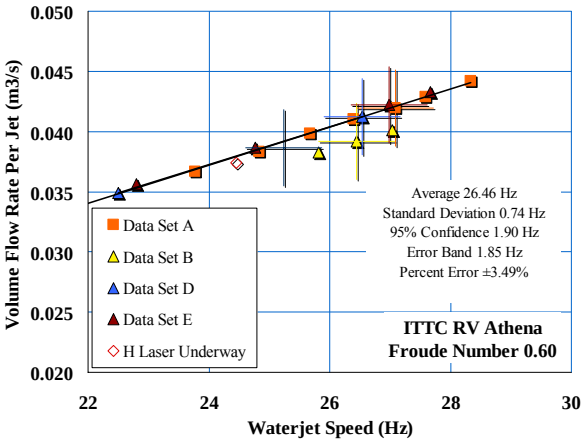

Figure 4.15- Comparison of reported model flow rate values for model self-propulsion point at Fn =0.60.

Figure 4.15 zooms in on the predicted flow rates, and shows the variation in the reported self-propulsion points for a Froude Number of 0.60. There appears to be a 3.5% maximum deviation from the mean in the estimation of model waterjet speed for the self-propulsion point.

The correspondence in flow rate assessment between data sets A, D and E is surprisingly good, however. The maximum deviation for a fixed impeller rate is well within 0.2%. The deviation between the mean of these three data sets and the LDV determined flow rate H amounts to 0.84%.

From the analysis of the propulsion test results, it appeared that the major problems were due to the post processing of data, rather than in the experiments themselves. Table A2, as found in Appendix A, gives a sample of the values reported used as input in the powering computations.

The first problem apparent from this table is the scatter in the tow force selected. There is a spread of 44.6%. Some differences are expected due to different water temperatures and correlation allowances but this would only account for 15% of the scatter.

It appears that although the relation between impeller speed and flow rate under-way has been determined consistently, the impact of an improper estimate of the operating point on the final result propagates by the second and third power in thrust and jet system power respectively. The scatter in the estimated model thrust is consequently some 18%.

At this point it is unclear if the respondents applied the corrections c_m and c_e for the non-uniformity of the flow in the inlet and jet flow (see Eqs. 3.16, 3.28 and 3.29). There was not enough information provided to determine this. However, considering the fact that those who did expand the data to full scale, often used the same IVR and NVR for both model (Table A2) and full size (Table A3) it is strongly suspected that these corrections were not applied.

The scatter in IVR at Station 1A was 7.6%. Every data set, except for data set H, had the same reported IVR for model and ship. The scatter in the NVR, showed a bandwidth of 4.7 %. The Nozzle Velocity Ratio NVR was used as an estimate for the Jet Velocity Ratio, since no one really estimated the effect of the vena contracta,

For data set H, two extrapolations are provided. One where the conventional thrust identity is used to determine the tow force accounting for the difference in friction between model and ship and the correlation allowance. In this case the IVR and NVR model and ship should be different due to the scaling and change in boundary layer velocity profiles. In the other case the tow force was determined using flow rate identity. Here the flow rate or NVR is assumed to be scaled so there is essentially no difference between model and ship values (Tables A2 and A3).

Summarizing, it does appear that there is no universal extrapolation method used in all data sets to convert the model scale values to full scale equivalents. The most important problem is the determination of the point for self-propulsion of the ship. The differences in the determination of this operating point over shadow any other differences, such as found in the flow rate or in the shape of the velocity profile and capture area.

Full-Scale Predictions. Every participant did not attempt a prediction of full-scale performance. An attempt was made by the Committee to do so, however, as noted in Tables A3 and A4 the Committee had to make assumptions on data where they were not provided. With this reservation, the estimation of full-scale resistance showed a maximum deviation of the mean of 6.6% (compared to 4.5% for the model values).

It appears that at a Froude Number of 0.60, the heave displacement measured at midship is 5 mm deeper (0.04 m full scale) with a working jet than bare hull. The running trim angle appears to be the same within the uncertainty of these measurements.

The maximum deviation from the mean in the reported ship scale waterjet speed is the same as for the model at a value of 4.5%. It was debated whether it is appropriate to even report the value of waterjet impeller speed. It was decided to do so for the purpose of pointing out that the final jet speed would, in all probability, not be Froude scalable from the model result. Especially the differences in the inlet velocity field will prevent similitude. The goal of the momentum flux method is to provide the flow rate and head rise required so that these results can be fed in the jet system characteristics to determine the final impeller speed and power P_D.

The biggest problem appeared to be the determination of the point to use for self-propulsion. It also appeared that accounting for the Reynolds Number scaling in the ingested momentum and energy fluxes is not universally used.

4.4 Conclusions

The results received indicate that the mechanics of the experimental procedures applied for the submitted data sets were generally sound. The biggest error is caused by deviations in the "self-propulsion point ship" at which the model is to be tested, defined by tow force F_D.

A (known) problem occurred in the scatter of the resistance test results (bandwidth 9% for all results). It is likely that blockage and/or shallow water effects in the facility are responsible for this large scatter.

The results of the viscous velocity profile with closed intakes at station 1A showed a remarkable correspondence. For the Athena model, a transverse variation in the boundary layer velocity profile could not be discerned, allowing the determination of ingested momentum and energy fluxes to be based on only a single boundary layer profile measurement. This measurement is preferably taken on the centreline of the intake to account for possible transverse variations.

The results of the velocity profile in the nozzle discharge area show a much greater scatter, due to the difficulty of measuring this profile adequately. The bandwidth in results appeared to be some 7% after removal of the outliers. It is noticed that small changes in longitudinal position of the measuring plane may cause large variations in velocity.

The shape of the capture area at station 1A for the Athena was concluded to be elliptical, based upon CFD analysis. Although it appears that shape does not have a significant effect on ingested momentum and energy flux (van Terwisga et al. (2002)). If no detailed information is available, it is recommended to use an elliptical capture area with a width that is 50% larger than the geometrical intake width at station 1.

A proven method and possibly the most practical method for flow rate measurement is based on the determination of the flow rate from bollard pull results applying an averaging reference pressure transducer in the jet system. The bollard pull jet thrust should be referred to the pressure differential of an averaging reference probe. The flow rate can subsequently be obtained from the measured jet thrust.

The scatter in flow rate for equal impeller speed appeared to result in a bandwidth of some 0.8% for four returned data sets. It should be realized here that the error in flow rate propagates with roughly a factor 2 in the error in thrust (sensitivity of error in thrust for an error in flow rate, Fig. 3.3). This error in flow rate is the most important contribution to the uncertainty in the final power prediction (see

also ITTC Procedure 7.5-02-05-03.3 "Uncertainty analysis - Example for propulsion test")

Of all the methods used to determine flow rate directly, the most accurate and repeatable was the use of a high density laser doppler survey at the inlet opening or internal to the waterjet system. The low uncertainty in flow rate does not necessarily imply a similar quality of the derived jet thrust. Additional uncertainties are introduced by possible air suction through the waterjet (uncertainty in spec. mass), velocity distribution in the jet and a difference between vena contracta and nozzle discharge area.

It appeared that many of the respondents did not account for the fact that the local velocity appears squared and cubed in respectively the momentum and power equations. This means that velocity correction terms need to be applied to the outgoing and ingoing fluxes, when using averaged velocities based on flow rate and local cross section.

It is recommended that the self-propulsion point for the model should be based on thrust identity, as is done with model tests on propeller driven vessels. It is, however, to be investigated whether a model operating condition based on flow rate identity would give better results. The rationale for this is that the flow rate affects the flow and the pressure distribution in the afterbody more than the thrust vector acting on the jet system. A small deviation in the thrust vector (which is inevitable when applying flow rate identity), is expected to only have a negligible effect on trim and sinkage in most cases.

5. RESULTS OF WATERJET SYSTEM AND PUMP TESTS

5.1 Background

The main purpose of the standardization test on the pump characteristics is to obtain sets of systematic model waterjet pump data from different laboratories and cross validate the results so that they can be used in the full-scale powering prediction of a waterjet propelled craft. Three laboratories performed these tests and the results are presented in Section 5.2.

The main purpose of the waterjet system test is to include the influence of the non-uniformities in the inflow to the pump on the pump performance. The joint inlet-pump performance (or jet system performance) can also be determined from this test. Two laboratories performed these tests and a selection of the results are shown in Section 5.3.

The experimental data on which this report is based, can be downloaded from the ITTC Waterjet Committee Web Site at www.ittc-wjc.insean.it.

5.2 Pump Tests

Presentation and Discussion of Data. The pump characteristics in terms of flow rate, head and torque were non-dimensionalized with pump diameter and rotational speed yielding the following coefficients:

- Flow rate coefficient:

$$K_{QJ} = \frac{Q_J}{\rho n D^3} \tag{5.1}$$

- Head coefficient:

$$K_H = \frac{gH_{35}}{n^2 D^2} \tag{5.2}$$

- Torque coefficient

$$K_Q = \frac{Q}{\rho n^2 D^5} \tag{5.3}$$

The measured non-dimensional head-flow curve for the waterjet pump is shown in Fig. 5.1 along with computational results using the Navier-Stokes code ANSYS-CFX 5.7 using the SST (Shear Stress Transport) turbulence model with a grid of about 100,000 cells. The head rise between stations 3 and 5 was computed from velocity and pressure surveys from hub to

tip. The measurements were taken at 4 or 5 angular locations and from 7 to 20 radial locations during the pump loop test

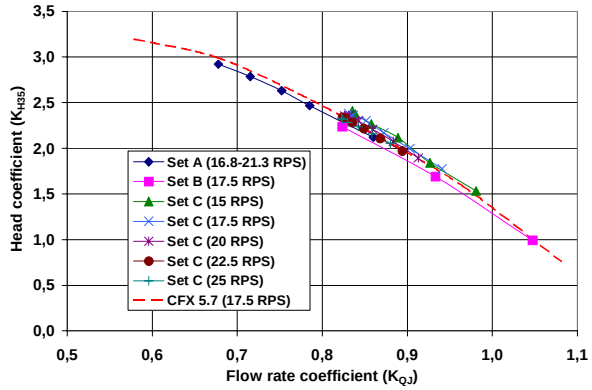

Figure 5.1- Non-dimensional head-flow curve for model waterjet pump.

The RPM was held constant for data sets B and C and the flow rate varied, whereas, data set A the flow rate was held constant and the RPM varied. The results follow the same general trend with the results from data set C slightly higher than data sets A and B. The computational results also show good agreement with the measured data. All measurements and computations were performed in non-cavitating conditions.

The measured and computed non-dimensional torque-flow curve for the waterjet pump is shown in Fig. 5.2. Again data set C shows higher values than data sets A and B.

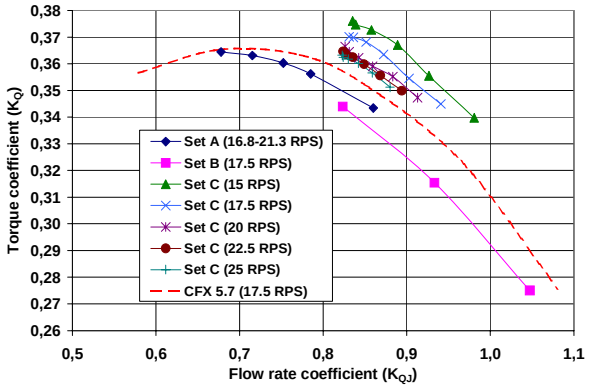

Figure 5.2- Non-dimensional torque-flow curve for model waterjet pump.

The measured and computed non-dimensional pump efficiency - flow curve for the waterjet pump is shown in Fig. 5.3.

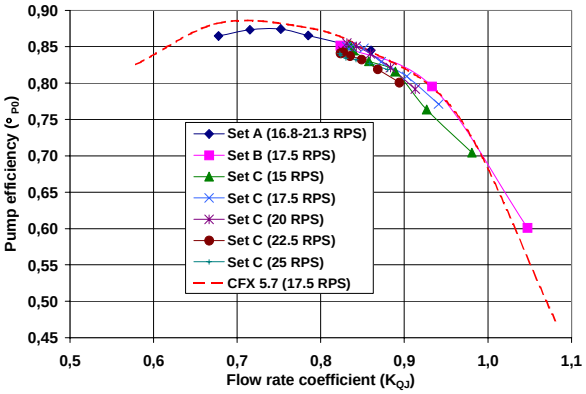

Figure 5.3- Non-dimensional pump efficiency-flow curve for model waterjet pump.

Taking all the data from the three laboratories and plotting them together, we obtain the best estimate of the characteristics for the model waterjet pump. Figure 5.4 shows the non-dimensional head-flow curve using all the data points. The following equation is the best-fit head-flow curve for this waterjet pump:

$$K_{H_{35}} = -6.4703 * K_{QJ}^2 + 6.12 * K_{QJ} + 1.7103$$

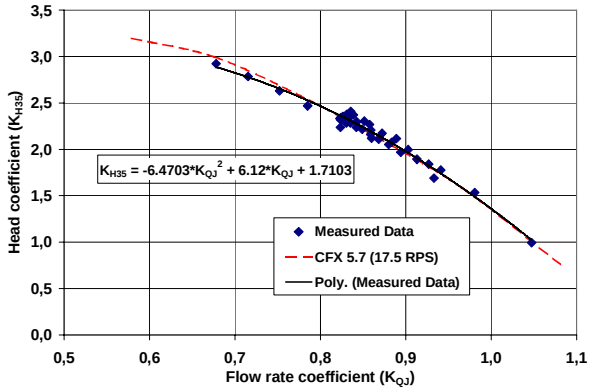

Figure 5.4- Non-dimensional head-flow data with curve fit.

Likewise the torque-flow data can be plotted for all three data sets as shown in Fig. 5.5. The best-fit curve is as follows:

$$K_Q = -1.1373 * K_{QJ}^2 + 1.7754 * K_{QJ} - 0.3255$$

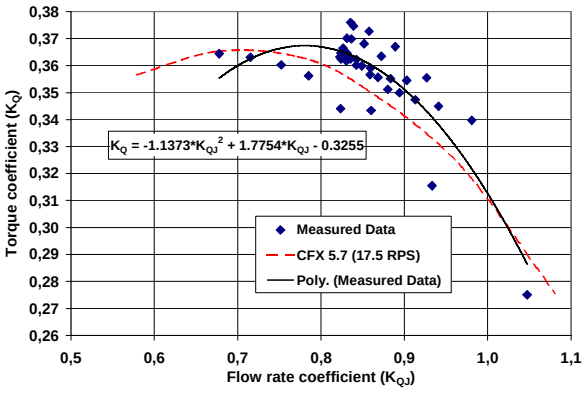

Figure 5.5- Non-dimensional torque-flow data with curve fit.

The pump efficiency and flow data sets can also be plotted together as shown in Fig. 5.6. The best-fit curve is as follows:

$$\eta_{PO} = -2.7843 * K_{QJ}^2 + 4.1317 * K_{QJ} - 0.6621$$

Once the required flow rate and effective jet system power P_{JSE} are known from the waterjet self-propulsion test, and the intake head loss has been assessed, the operating point of the pump of the pump can be determined. This will consequently result in head rise, torque and pump efficiency.

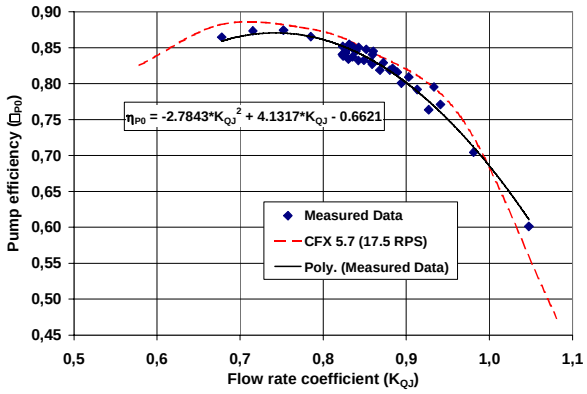

Figure 5.6- Non-dimensional pump efficiency-flow data with curve fit.

Conclusions. The returned three data sets indicate a good correlation both in terms of head and torque, as in terms of efficiency versus flow rate. In terms of pump efficiency they are within ±2%. The following important issues should be considered in conducting the tests and in processing the data:

1. The derived pump head should be based on axial dynamic head and not on total dynamic head. This is because the tangential and radial components do not contribute to the waterjet thrust and hence should not be incorporated in the computation of pump head and efficiency.
2. Velocity and pressure surveys with three hole or five hole probes should be performed at the outlet of the pump stage so that the exact magnitude of dynamic head associated with axial velocity can be derived.
3. The inlet flow to the pump should normally be fairly uniform in the pump loop test. However, an inlet survey is considered necessary to ensure the uniformity of the inflow velocity to the pump.

The computational curves also agree well with the best-fit curves for this data set and shows promise that using a less expensive computational method may provide similar results in estimating the pump performance.

5.3 Waterjet System Tests

Presentation and Discussion of Data. Two laboratories that performed the pump test, also performed the waterjet system test. They are again referred to as data sets A and C. The results presented here are in the same non-dimensional form as in Section 5.2. The same computational results as presented in Section 5.2 are also shown here, together with the system test results. No computations were, however, done for the complete jet system (joint inlet-duct system).

Figure 5.7 shows the head-flow curve for the pump. Data set A shows significantly higher values than in the pump test, possibly explained by the fact that no velocity surveys were done. Data set C is closer to the pump loop test results.

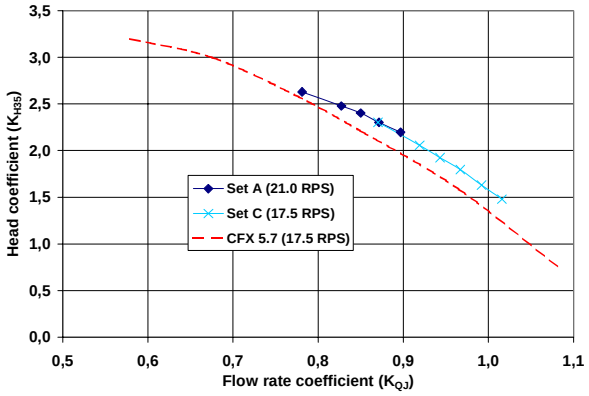

Figure 5.7- Non-dimensional head-flow curve for model waterjet pump.

Figure 5.8 shows the torque-flow curve. Both data set A and C show lower values than corresponding pump loop test results.

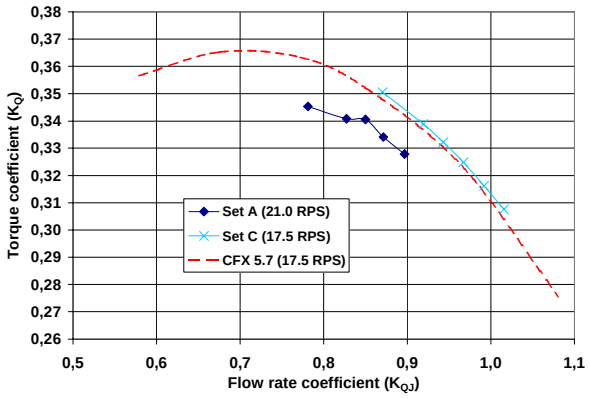

Figure 5.8- Non-dimensional torque-flow curve for model waterjet pump.

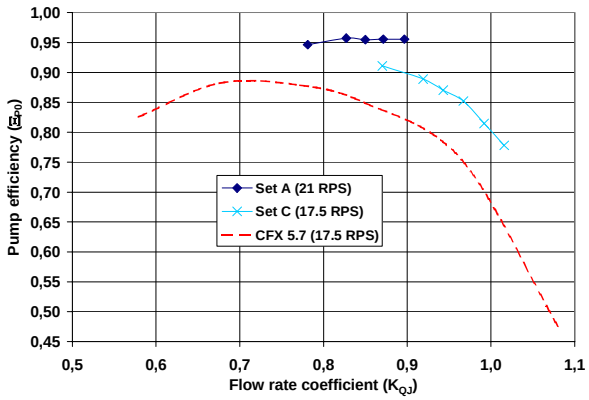

Figure 5.9- Non-dimensional pump efficiency-flow curve for model waterjet pump.

Figure 5.9 finally shows the pump efficiency-flow curve. The difference between pump efficiency obtained in a system test and pump efficiency obtained in a pump loop test should be a measure for the influence of the non-uniformities in the inflow to the pump. Figure 5.9, however, shows that the pump efficiencies measured in the system test were 5-10% higher than in the pump loop test.

Conclusions. Results from the system test show difficulties in obtaining pump efficiency from a system test. The expected small drop in efficiency was not seen, but instead a large increase in efficiency occurred. The derived head seems to be the greatest contributor to this unexpected result. Furthermore, the level of the torque measurement of data set C is yet unexplainable.

The discrepancy between pump efficiency from pump tests and from waterjet system tests is accounted for by a so called installation efficiency. This efficiency accounts for the interaction between the intake flow and the pump performance. Determination of the installation efficiency requires velocity and pressure surveys to be performed both upstream and downstream of the pump unit. The downstream measurement is quite straightforward while the upstream measurement is much more difficult. Using mean values of velocity and pressure based on flow rate, sectional area and wall pressure is not recommended since it may introduce errors in head and efficiency exceeding 5%.

It can be argued that the jet system characteristics in terms of K_{H1A7}, K_Q and K_{QJ} can be more accurately determined than the pump characteristics (i.e. excluding the intake losses), in case no detailed velocity and pressure surveys are available for the pump inlet plane (at station 3).

It is recommended to simulate the full-scale boundary layer in the model test, if the difference to full-scale can be expected to have a significant influence on the inlet duct flow and

therefore on the system performance. This scaling of the boundary layer may, however, not always be possible.

6. CONCLUSIONS AND RECOMMENDATIONS

6.1 Conclusions

Conclusions on Performance Prediction Method. A systematic breakdown of elements of the waterjet-hull system is made. A control volume representing the waterjet system is defined and the conservation laws of mass, momentum and energy are subsequently applied. This leads to a set of relations where the overall powering characteristics is explicitly expressed as the product of free stream characteristics and waterjet-hull interaction. A physical interpretation of the jet-hull interaction is presented.

Conclusions from Standardization Tests. The following conclusions from the standardization tests are based on seven returned data sets (aspiration level 7) and three pump test data sets (aspiration level 5) as well as two waterjet system data sets (aspiration level 5). Despite the fact that the aspiration levels for the pump tests and waterjet system tests were not met, the collected results are regarded sufficient to draw the following conclusions.

Resistance Test Results. The difference between minimum and maximum measured resistance appeared to be some 9%. The cause for the scatter in the resistance tests is largely known and reported in ITTC (Taniguchi, 1963). This discrepancy is not expected to lead to differences in thrust deduction, because it is assumed that the same systematic error is present during the propulsion test.

Possible causes that do affect the value of the thrust deduction and that are unique to waterjet propelled craft are:

- Discrepancies in the displacement weight and LCG accounting for the waterjet entrained water during the resistance test.
- Possible change of displacement weight during tests due to leaking of water through the inlet and nozzle covers.
- Possibility of parasite drag due to the presence of a velocity probe for boundary layer velocity measurement.

Flow Rate Measurement. A proven method and possibly the most practical method is based on the determination of the flow rate from bollard pull results, applying an averaging reference pressure transducer in the jet system. The bollard pull jet thrust should be referred to the pressure differential of an averaging reference probe. The flow rate can subsequently be obtained from the measured jet thrust.

Of all the methods used to determine flow rate directly, the most accurate and repeatable was the use of a high density laser doppler survey at the inlet opening or internal to the waterjet system. Less reliable measurements were obtained with filling a volume or from integration of velocity surveys using a pressure based velocity survey.

Ingested Momentum and Energy Flux. The measured boundary layer profile appeared to be insensitive to the longitudinal position for the closed intake. This is not the case for an open inlet with working waterjet. The boundary layer profile should be measured, by convention, in station 1A, which is defined as the location that is one impeller diameter forward of the ramp tangency point (station 1). It should further be measured with intake openings closed (nominal wake field).

No significant differences were measured in the normalized boundary layer profile for different transverse locations at station 1A, although there were differences in the boundary layer height. These differences did, however, not significantly effect the estimated flow coefficients as compared to the analysis with a

single centreline velocity profile, when an elliptical capture area was used.

The exact shape of the capture area at station 1A does have a small effect on ingested momentum and energy flux. If no detailed information is available, it is recommended to use an elliptical capture area with a width that is 50% larger than the geometrical intake width at station 1. The use of an elliptical capture area reduces the effects of any transverse variation in the velocity profile.

Discharged Momentum and Energy Flux. The differences in measured jet profile were significant. This measurement appeared to be very sensitive to longitudinal and angular location (due to the wake of the stator and skewed intake flow). This is illustrative for the difficulty of this measurement.

Determination of Tow Force. It is recommended that the tow force during the model propulsion tests is determined from thrust identity (i.e. equal thrust coefficient for ship and model) until a procedure based on flow rate identity has proven more successful.

Pump Tests. The returned three data sets indicate a good correlation both in terms of head and torque, as in terms of efficiency versus flow rate. The following important issues should be considered in conducting the tests and in processing the data:

1. The derived pump head should be based on axial dynamic head and not on total dynamic head.
2. Velocity and pressure surveys with three hole or five hole probes should be performed at the outlet of the pump stage so that the exact magnitude of dynamic head associated with axial velocity can be derived.
3. The inlet flow to the pump should normally be fairly uniform in the pump loop test.

Waterjet System Tests. The conclusions on the standardisation test for the complete Waterjet System are based on 2 sets of data.

The installation efficiency accounts for the interaction between the intake flow and the pump performance. Determination of the installation efficiency requires velocity and pressure surveys to be performed both upstream and downstream of the pump unit. Using mean values of velocity and pressure based on flow rate, sectional area and wall pressure is not recommended since it may introduce errors in head and efficiency exceeding 5%.

It is recommended to simulate the full-scale boundary layer in the model test, if the difference to full-scale can be expected to have a significant influence on the inlet duct flow and therefore on the system performance. This scaling of the boundary layer may, however, not always be possible.

6.2 Recommendations

Adopt the new Procedure: 7.5-02-05-03.1 Testing and Extrapolation Methods - High Speed Marine Vehicles, Waterjets Propulsive Performance Prediction.

Adopt the new Procedure: 7.5-02-05-03.2 Testing and Extrapolation Methods - High Speed Marine Vehicles, Waterjets - Waterjet System Performance.

Adopt the new Procedure: 7.5-02-05-03.3 Testing and Extrapolation Methods - High Speed Marine Vehicles, Waterjets Uncertainty Analysis - Example for Propulsion Test.

7. REFERENCES

Aartojärvi, R., Header, M., Lundberg, J. and Seil, G. J., 2004, “Implementation of Result of CFD Analysis to the Design of a New Waterjet Steering and Reversing Unit”,

International Conference on Waterjet Propulsion 4, RINA, London, UK, pp. 1-9.

Altosole, M., Benvenuto, G., Figari, M. and Compora, U., 2004, "Performance Prediction of a Waterjet Propelled Craft by Dynamic Numerical Simulation", International Conference on Waterjet Propulsion 4, RINA, London, UK, pp. 75-84.

Bowles, J.B. and Schleicher, D.M., 2004, "Tradeoffs Between Two and Three Waterjets on Fast Planning Monohulls", International Conference on Waterjet Propulsion 4, RINA, London, UK, pp. 47-65.

Buckingham, J.E., 2004, "Modelling of Waterjets in a Propulsion System", International Conference on Waterjet Propulsion 4, RINA, London, UK, pp. 85-93.

Bulten, N.W.H. and Verbeek, R., 2003 "Design of Optimal Inlet Duct Geometry Based on Vessel Operational Profile", International Conference on Fast Sea Transportation, Vol. I, Ischia, Italy, pp. 35-40.

Bulten , N.W.H. and Verbeek, R., 2004, "CFD Simulations of the Flow Through a Waterjet Installation", International Conference on Waterjet Propulsion 4, RINA, London, UK, pp. 11-19.

Carlton, J.S., 2002, "Waterjet Propulsion: Some Recent Full Scale Experience", The 2nd PNU International Colloquium on Waterjet, Busan, Korea, pp. 129-134.

Choi, G.I. and Ahn, Y.W., 2002, "The Generation of Waterjet Inlet Geometry Using NURBS", The 2nd PNU International Colloquium on Waterjet, Busan, Korea, pp. 105-110.

Chun, H. H., Kim, M. C. Ahn, B. H. and Cha, S. M., 2003, "Self-propulsion Test and Analysis of an Amphibious Tracked Vehicle with Waterjet", SNAME Symposium, St. Francisco, USA.

Etter, R.J., Krishnamoorthy, V. and Scherer, J.O.; "Model testing of waterjet propelled craft", Proceedings of the 19th ATTC, 1980.

Facinelli, W.A., Becnel, A.J., Purnell, J.G. and Blumenthal, R.F., 2003, "Design of an Advanced Waterjet", SNAME Propeller/Shafting '03 Symposium, Virginia Beach, Virginia, pp. 7-1~7-9.

Hoyt III, J.G. (Chairman), 1999, "Report of the Specialist Committee on Waterjet", 22nd ITTC, Seoul/Shanhai.

Kim, K.C., Yoon, S.Y., Jeong, E.H., Kwon, S.H., Chun, H.H. and Kim, M.C., 2002, "Measurement of Wall Pressure Distributions and Velocity Field of a Waterjet Intake Flow", The 2nd PNU International Colloquium on Waterjet, Busan, Korea, pp. 153-158.

Kim, M.C., Chun, H.H. and Park, W.G., 2003, "Design of an Waterjet Propulsion System for an Amphibious Tracked Vehicle", International Conference on Fast Sea Transportation, Ischia, Italy, pp. 35-40.

Kim, M. C., Chun, H. H., Park, W. G. and Byun, T. Y., 2004, "Study on a Pod Type Waterjet for an Amphibious Wheeled Vehicle", International Conference on Waterjet Propulsion 4, RINA, London, UK, pp. 101-110.

Kooiker, K., van Terwisga, T., Verbeek, R. and van Terwisga, P., 2003, "Performance and cavitation analysis of a waterjet system mounted on a cavitation tunnel", International Conference on Fast Sea Transportation, Ischia, Italy.

Kruppa, C. (Chairman), 1996, "Report of the Specilist Committee on Waterjets", 21st ITTC, Bergen and Trondheim, pp. 189-209.

Murrin, D.C., Bose, N. and Chin, S.N., 2004, "Waterjet System Wind Tunnel Test", Inter-

national Conference on Waterjet Propulsion 4, RINA, London, UK, pp. 21-28.

Park, W.G., Yun, H.S., Chun, H.H. and Kim, M.C., 2002a, "Numerical Analysis of Intake Flow of Waterjet Pump", The 2nd PNU International Colloquium on Waterjet, Busan, Korea, pp. 73-91.

Park, I.R., Kim, K.S., Lee, S.S. and Ahn, J.W., 2002b, "Numerical Simulation of Intake Duct Flow for a Waterjet Propulsor", The 2nd PNU International Colloquium on Waterjet, Busan, Korea, pp. 93-103.

Park, B.J., Lee, S.S., Kim, K.S. and Ahn, J.W., 2002c, "The Methodology for Geometric Modelling of Waterjet Intake Duct", The 2nd PNU International Colloquium on Waterjet, Busan, Korea, pp. 171-178.

Park, W.G. and Chun, H.H., 2002d, "Numerical Simulation of Flow Field of Waterjet Propulsion System", The 2nd PNU International Colloquium on Waterjet, Busan, Korea, pp. 51-65.

Savitsky, D. (Chairman), 1987, "Report of the High Speed Marine Vehicle Committee", 18th ITTC, pp. 304-313, Kobe, Japan.

Scherer, O., Mutnick, I. and Lanni, F.; "Procedure for conducting a towing tank test of a waterjet propelled craft using Laser Doppler Velocimetry to determine the momentum and energy flux", Proc. of the 26th ATTC, July 2001.

Seil, G., 2001, "Experimental Validation of the Calculated Flow in a Waterjet Steering and Reversing Unit", International Conference on Fast Sea Transportation, Southampton, UK, pp. 31-40.

Taniguchi, K., "The Resistance Tests on the ITTC Standard Model", 10th ITTC, Teddington, 1963.

van Terwisga, T.J.C., 1996, "Waterjet-Hull Interaction", PhD Thesis, Delft University of Technology, ISBN90-75757-01-8.

van Terwisga, T. and Alexander, K.V., 1995 "Controversial issues in Waterjet-Hull Interaction", International Conference on Fast Sea Transportation, Lubeck.

van Terwisga, T.J.C. (Chairman), 2002, "Report of the Specialist Committee on Validation of Waterjet Test Procedures", 23rd ITTC, Vol II, Venice.

Verbeek, R., 2002, "Waterjet Concepts for Fast Ships", The 2nd PNU International Colloquium on Waterjet, Busan, Korea, pp. 159-170.

Wang, Y., Ding, J., Ao, C. and Chen, H., 2004, "Research on the Relationship Between Waterjet Power Absorption and Vessel Speed", International Conference on Waterjet Propulsion 4, RINA, London, UK, pp. 39-45.

Wilson, M.B., Hoyt III, J.G., Scherer, J.O., Gorski, J.J. and Becnel, A.J., 2003, " The Gulf Coast Waterjet Design and Experimental Evaluation Project for a Small Navy Ship", SNAME Propeller/Shafting '03 Symposium, Virginia Beach, Virginia, pp. 18-1~18-19.

Wilson, M. B., Chesnakas, C., Gowing, S., Becnel, A. J., Purnell, J. G. and Stricker, J. g., 2004, "Analysis of Hull Boundary Layer Velocity Distributions With and Without Active Waterjet Inlets", International Conference on Waterjet Propulsion 4, RINA, London, UK, pp. 29-37.

Wilson, M.B., Gowing, S., Chesnakas, C.J. and Lin, C.W., "Waterjet-hull interactions for Sealift Ships", International Conference on Marine Research and Transportation, Ischia, Italy, 19-21 Sept. 2005.

APPENDIX A

Table A1- Comparison Of Bare Hull Resistance Results At A Froude Number Of 0.60.

Data Reported	Model Speed	Bare Hull Resistance	Model Heave	Model Trim	Water Temperature	Model Drag Coefficient	Model Reynolds No.	Model Friction Coef	Correlation Allowance	Model Weight	Ship Disp.
Froude Number	V_m	R_{TBHm}	z_{Mm}	θ_{vm}	t_{wm}	C_{Tm}	R_{nm}	C_{Fm}	C_A	kg	kg
0.6	m/s	N	m	deg	^{0}C						
Data Set A	4.399	284.08	-0.015	1.36	17.4	6.814E-03	2.249E+07	2.618E-03	4.00E-04	432.0	277,977
Data Set B	4.396	282.49	0.001	1.21	17.2	6.778E-03	2.241E+07	2.620E-03	4.00E-04	442.0	284,099
Data Set C	4.402	261.83	-0.011	1.36	20.4	6.274E-03	2.422E+07	2.586E-03	2.00E-04	414.3	266,687
Data Set D	4.397	268.71	-0.006	1.39	14.1	6.449E-03	2.067E+07	2.656E-03	3.70E-04	421.8	271,270
Data Set E	4.410	278.67	-0.006	1.34	16.0	6.650E-03	2.180E+07	2.632E-03	3.70E-04	-	-
Data Set H	4.401	260.25	-0.006	1.42	20.4	6.240E-03	2.428E+07	2.586E-03	1.70E-04	419.8	270,254
Data Set I	4.395	259.57	-0.004	1.14	19.0	6.239E-03	2.310E+07	2.601E-03	2.00E-04	421.6	271,367
Average	4.400	270.800	-0.007	1.317	17.786	6.492E-03	2.271E+07	2.614E-03	3.01E-04	425.2	273,609
Standard Deviation	0.005	10.780	0.005	0.102	2.324	2.541E-04	1.294E+06	2.532E-05	1.05E-04	10.01	6,306
95% Confidence	0.012	25.494	0.012	0.241	5.496	6.010E-04	3.060E+06	5.988E-05	2.49E-04	23.68	14,913
Error Band	0.015	24.510	0.016	0.280	6.300	5.747E-04	3.614E+06	6.976E-05	2.30E-04	27.70	17,412
Percent Error	±0.17%	±4.53%	±116.67%	±10.64%	±17.71%	±4.43%	±7.96%	±1.33%	±38.15%	±3.26%	±3.18%

Table A2- Comparison Of Model Momentum Results At A Froude Number Of 0.60.

Data Reported	Model Speed	Bare Hull Resistance	Conventional Tow Force	Reported Tow Force	Waterjet Speed	Volume Flow Rate	Estimated Total Thrust	Model Heave	Model Trim	Inlet Vel Ratio	Nozzle Vel Ratio
Froude Number	V_m	R_{TBHm}	ΔC_{Fm}	F_D	n_m	Q_{Jm}	T_m	z_{Mm}	θ_{vm}	IVR	NVR
0.6	m/s	N	N	N	Hz	m^3/s	N	m	deg	Sta. 1	Sta. 6
Data Set A	4.399	284.08	22.96	28.51	27.08	0.0420	294.90	-0.012	1.46	0.788	1.722
Data Set B	4.396	282.49	22.99	42.71	26.45	0.0392	262.19	0.000	1.25	0.826	1.587
Data Set C	4.402	261.83	30.01	-	25.18	-	247.63	-0.028	0.83	-	-
Data Set D	4.397	268.71	25.75	27.00	26.54	0.0413	305.80	-0.001	1.53	0.893	1.667
Data Set E	4.410	278.67	24.91	24.74	26.99	0.0422	317.56	-0.006	1.54	0.886	1.704
Data Set H ΔC_f	4.401	260.25	31.22	31.22	24.72	0.0378	219.00	-0.013	1.33	0.876	1.535
Data Set H BL Scl'd	4.401	260.25	31.22	17.19	25.23	0.0386	219.65	-0.013	1.33	0.921	1.568
Data Set I	4.395	259.57	30.50	-	25.67	-	-	-0.023	1.11	-	-
Average	4.400	269.481	27.443	28.561	25.983	0.0402	266.67	-0.012	1.3	0.865	1.631
Standard Deviation	0.005	10.654	3.657	8.407	0.898	0.0019	40.38	0.010	0.24	0.049	0.078
95% Confidence	0.011	25.197	8.649	19.884	2.125	0.0044	95.50	0.023	0.56	0.115	0.183
Error Band	0.015	24.510	8.260	25.514	2.361	0.0044	98.56	0.028	0.71	0.133	0.187
Percent Error	±0.17%	±4.55%	±15.05%	-±44.67%	±4.54%	±5.47%	±18.48%	±116.47%	±27.41%	±7.69%	±5.73%

Table A3- Comparison Of Ship Momentum Results At A Froude Number Of 0.60.

Data Reported	Ship Speed	Ship Inlet Mom. Speed	Ship Jet Mom. Speed	Inlet Vel Ratio	Nozzle Vel Ratio	Model Reynolds No.	Model Friction Coef	Model Drag Coefficient	Ship Resistance	Volume Flow Rate	Estimated Total Thrust
Froude Number	V_s	V_{im}	V_{jetm}	IVR	NVR	R_{nm}	C_{Fm}	C_{Tm}	R_{TBHs}	Q_{Jm}	T_m
0.6	m/s	m/s	m/s	Sta. 1	Sta. 6				N	m^3/s	N
Data Set A	12.867	10.135	22.157	0.788	1.722	5.083E+08	1.668E-03	6.263E-03	168,087	9.118	193,872
Data Set B	12.858	10.620	20.405	0.826	1.587	5.079E+08	1.668E-03	6.227E-03	166,791	8.393	168,504
Data Set C	12.876	-	-	-	-	5.086E+08	1.667E-03	5.555E-03	149,221	-	159,400
Data Set D	12.860	11.483	21.440	0.893	1.667	5.080E+08	1.668E-03	5.831E-03	156,251	8.819	196,674
Data Set E	12.899	11.424	21.983	0.886	1.704	5.095E+08	1.667E-03	6.056E-03	163,246	9.042	195,885
Data Set H ΔC_f	12.873	11.856	20.172	0.921	1.567	5.085E+08	1.668E-03	5.492E-03	147,450	8.272	141,147
Data Set H BL Scl'd	12.873	11.856	20.185	0.921	1.568	5.085E+08	1.668E-03	5.492E-03	147,450	8.276	141,428
Data Set I	12.856	-	-	-	-	5.078E+08	1.668E-03	5.506E-03	147,434	-	-
Average	12.870	11.229	21.057	0.872	1.636	5.084E+08	1.668E-03	5.803E-03	155,741	8.653	170,987
Standard Deviation	0.014	0.701	0.915	0.054	0.070	5.469E+05	3.107E-07	3.380E-04	9,103	0.387	24,860
95% Confidence	0.033	1.657	2.163	0.128	0.167	1.293E+06	7.347E-07	7.994E-04	21,530	0.916	58,793
Error Band	0.043	1.721	1.985	0.133	0.155	1.698E+06	8.780E-07	7.716E-04	20,653	0.846	55,527
Percent Error	±0.17%	±7.66%	-±4.71%	±7.64%	±4.74%	±0.17%	±0.03%	±6.65%	±6.63%	±4.89%	±16.24%

NOTE: Not Reported, Calculated with best available information when received.

Table A4- Comparison Of Full Scale Prediction At A Froude Number Of 0.60.

Data Reported	Ship Speed	Ship Resistance	Ship Heave	Ship Trim	Waterjet Speed	Volume Flow Rate	Nozzle Vel Ratio	Estimated Total Thrust	Ship Power	Thrust Deduction	Jet Efficiency
Froude Number	V_s	R_{TBHs}	z_{Mm}	θ_{vm}	n_m	Q_{Jm}	NVR	T_m	P_{JSE}	t	η_{JSE}
0.6	m/s	N	m	deg	Hz	m^3/s	Sta. 6	N	Kw		
Data Set A	12.867	168,087	-0.103	1.46	9.26	9.118	1.722	193,872	3284.6	0.133	0.658
Data Set B	12.858	166,791	0.000	1.25	9.04	8.393	1.587	168,504	2614.3	0.010	0.820
Data Set C	12.876	149,221	-0.239	0.83	8.61	-	-	148,183	4028.3	-0.007	0.477
Data Set D	12.860	156,251	-0.005	1.53	9.07	8.819	1.667	196,674	2971.4	0.206	0.676
Data Set E	12.899	163,246	-0.055	1.54	9.23	9.042	1.704	195,885	3272.0	0.167	0.644
Data Set H ΔC_f	12.873	147,450	-0.111	1.33	8.45	8.272	1.567	141,147	2289.1	-0.045	0.829
Data Set H BL Scl'd	12.873	147,450	-0.111	1.33	8.63	8.276	1.568	141,428	2296.6	-0.043	0.827
Data Set I	12.856	147,434	-0.197	1.11	8.78	-	-	-	-	-	-
Average	12.870	155,741	-0.103	1.30	8.883	8.653	1.636	169,385	2,965.2	0.060	0.704
Standard Deviation	0.014	9,103	0.084	0.24	0.307	0.387	0.070	26,063	626.3	0.105	0.131
95% Confidence	0.033	21,530	0.200	0.56	0.726	0.916	0.167	61,640	1,481.2	0.249	0.309
Error Band	0.043	20,653	0.239	0.71	0.807	0.846	0.155	55,527	1,739.2	0.250	0.352
Percent Error	±0.17%	±6.63%	±116.5%	±27.41%	±4.54%	±4.89%	±4.74%	±16.39%	±29.33%	±207.95%	±25.00%

NOTE: Not Reported, Calculated with best available information when received.